Single-cell RNA Sequencing Technology Revealed the Pivotal Role of Fibroblast Heterogeneity in Ang II-Induced Abdominal Aortic Aneurysms

Yingzheng Weng
Zhejiang Hospital https://orcid.org/0000-0003-0671-6782
Jiangjie Lou
Zhejiang Hospital
Yizong Bao
Zhejiang Hospital
Changhong Cai
Lishui Central Hospital and Fifth Affiliated Hospital of Wenzhou Medical College
Kefu Zhu
Zhejiang Hospital
Changqing Du
Zhejiang Hospital
Xiaofeng Chen
Taizhou Hospital
Lijiang Tang (zjyytang@163.com)
Zhejiang Chinese Medical University https://orcid.org/0000-0001-6005-3612

Research

Keywords: abdominal aortic aneurysm, Single cell RNA sequencing, fibroblast, Cell communications

Posted Date: November 2nd, 2021

DOI: https://doi.org/10.21203/rs.3.rs-970793/v1

Abstract

Aim: The mechanism of abdominal aortic aneurysm (AAA) has not been fully elucidated. In this study, we aimed to map the cellular heterogeneity, molecular alteration, and functional transformation of angiotensin (Ang) II-induced AAA in mice based on single-cell RNA sequencing (sc-RNA seq) technology.

Method: Single-cell RNA sequencing was performed on suprarenal abdominal aorta from male APOE-/- C57BL/6 mice of Ang II-induced AAA and shame models. Immunohistochemistry was used to determine the pathophysiological characteristics of AAA, and sc-RNA seq was used to determine the heterogeneity and phenotypic transformation of all cell types. A single-cell trajectory was performed to predict the differentiation of fibroblasts. Finally ligand–receptor analysis was used to evaluate intercellular communication between fibroblasts and smooth muscle cells.

Results: More than 27,000 cells were isolated and 25 clusters representing 8 types of cells were identified, including fibroblasts, macrophages, endothelial cells, smooth muscle cells, T lymphocytes, B lymphocytes, granulocytes, and natural killer cells. During AAA progression, the function and phenotype of different type cells altered separately. The pro-inflammatory function of inflammatory cells was enhanced. The proliferation phenotype degreased while pro-inflammatory, regeneration and damage-related phenotypes increased in endothelial cells. Smooth muscle cells also transformed from contractile to secretory phenotype. The alterations of fibroblasts were the most conspicuous according sub-group clustering analysis. Single-cell trajectory revealed the critical reprogramming genes of fibroblasts mainly enriched in regulation of immune system. Finally, the ligand–receptor analysis confirmed that increases in secondary collagen synthesis led by fibroblasts were one of the most prominent characteristics of Ang II-induced AAA.

Conclusion: Our study revealed the cellular heterogeneity of Ang II-induced AAA. Fibroblasts may play a central role in Ang II-induced AAA progression according multiple biological functions including immune regulation and extracellular matrix metabolic balance. Our study may provide us with a different perspective on the etiology and pathogenesis of AAA.

1. Background

Abdominal aortic aneurysm (AAA) is a common fatal cardio great vessel disease worldwide, characterized by a degree of local dilation ≥ 50% compared with that of adjacent normal tissue [1]. Although research on AAA has been ongoing for decades, it's etiology remains controversial [2, 3]. Currently, there are several hot topics surrounding the pathogenesis of AAA. 1) The connection between AAA and atherosclerosis: Conventional view was that AAA was just a result/manifestation of atherosclerosis. However, researchers found that AAA seems to be independent of atherosclerosis, from the perspective of clinical, genetic, and biochemical studies in recent years [3]. It is unquestionable that both AAA and atherosclerosis share some common pathophysiological characteristics, such as chronic vascular inflammation, vascular remodeling, and involvement of the renin-angiotensin-aldosterone

system (RAAS) [4]; however, diabetes appears to be a protective factor for AAA formation, unlike atherosclerosis [5]. 2) Association between dynamic balance of extracellular matrix (ECM) metabolism and the onset of AAA: Degradation of the ECM has been confirmed to be one of the most prominent characteristics of AAA. However, synthesis and degradation of extracellular matrix is a complex and dynamic process required studies in detail. Collagen, one of the ECM proteins, plays a major role in the repair of arteries. Some researches indicted that an increase in collagen can lead to stiffening of the arterial wall, causing a susceptibility to rupturing and aortic dissection. By contrast, loss of collagen contributes to the formation of AAA [6]. The dynamic changes of ECM metabolism are important factors for predicting the prognosis of AAA. In a word, the pathogenesis and pathophysiology of AAA have not been fully elucidated. Further exploration on the pathogenesis of AAA is of great value.

Arterial wall tissue is composed of cells with different functions. The potential molecular and cellular heterogeneity are critical for the progression of AAA and remain poorly understood. Conventional genomics and proteomics only analyze the pathogeneses of diseases at the organizational level [7, 8]. The emergence of single-cell RNA sequencing (sc-RNA seq) technology has provided new opportunities for research. It reveals the heterogeneity of complex cell populations and intercellular interaction according to pivotal characteristic genes.

There were three classic mouse AAA models commonly used in the laboratory, including porcine pancreatic elastase-induced AAA models, Ang II-induced AAA models, and calcium chloride ($CaCl_2$)-impregnated AAA models [9]. All three have their own advantages and disadvantages, and a comprehensive study of AAA using different models is necessary. Existing studies had shown that the pathological changes of elastase-induced AAA were most similar to those in human AAA [10]. The basic principle of this model is to degrade the middle elastin and reduce the ability to withstand the stress of the blood vessel wall. Apoptosis of smooth muscle cell, infiltration of inflammatory cell and deposition of collagen fibers gradually emerge, which produces AAA-like expansion. Zhao et al explored the changes in transcription signals at the individual cell level in pancreatic elastase-induced AAA models [11]. The study described that the number of cells with a normal tissue structure, including smooth muscle cells (SMCs) and endothelial cells (ECs), decreased continuously, while inflammatory cells continuously infiltrated the artery wall tissue during the process of AAA formation. However, hyperlipidemia, one of the risk factors for AAA in humans, does not affect development of elastase-induced AAA in mice [12]. Human AAA is often accompanied by calcification, so there are certain similarities in pathological features of $CaCl_2$-impregnated AAA compared with human AAA. The specific mechanism is the destruction of the ECM and endothelial cell damage caused by calcium deposition. The infiltrating Ca^+ accelerates the infiltration of inflammatory cells and the expression of matrix metalloproteinases (MMPs), which ultimately leads to the formation of AAA [13]. Ang II-induced AAA is comparable to human AAA to some extent. ECM degradation, inflammatory cell infiltration, compensatory deposition of collagen and angiogenesis are also its characteristic performance. What's more, some high-risk factors of human AAA, such as gender, age, smoking, hypercholesterolemia, can significantly promote the occurrence and progress of AAA in this model. However, it mainly forms aortic dissection aneurysm (ADA), which is not exactly the same as true

aneurysm [14]. A single model can only reflect one aspect of the AAA. Previous studies have explored the cellular heterogeneity of elastase-induced AAA and $CaCl_2$-impregnated AAA models [11, 15]. Mapping the cellular heterogeneity of Ang II-induced AAA in mice will complete the research on the mechanism of the disease. Transcriptome sequencing of Ang-II-induced AAA at the single-cell level may become one piece of the puzzle in the on the mechanism researches of AAA.

In this study, we constructed Ang II-induced AAA models for 10x Genomics sc-RNA seq to analyze the cellular heterogeneity and molecular alterations of the disease which may be complement genetic studies of aortic disease. Our research might provide different perspectives for understanding AAA progression.

2. Methods

2.1 Animals and rearing condition

A total of 30 male *Apoe-/-* C57Bl/6J mice (10 weeks) (purchased from GemPharmatech Co., Ltd, Soochow, China) were used for the experiments. All mice were raised in the specific pathogen free (SPF) laboratory of Zhejiang Academy of Medical Sciences and were randomly divided into two equal groups (n = 15), namely, the control (CTR) group and the AAA group. Mice were housed communally with a standard 12 h dark cycle and fed ad libitum. The room temperature was controlled at 20–25 ℃, and the humidity was controlled at 50–60%. All our operations were in line with“Guiding Principles in the Care and Use of Animals” (China). Ethics approval was obtained from laboratory of Zhejiang Academy of Medical Sciences (No. 20200271) prior to the start of the study.

2.2 Construction of AAA models

All of the mice were used for model construction after 2 weeks of adaptation and pre-feeding. To generate the model, the AAA group was administered Ang II solution (1000 ng/kg/min, Sigma Chemical Co., St Louis, MO, USA) via Alzet osmotic minipumps 2004 (Durect Corporation, Cupertino, USA), while the CTR group was administered normal saline for 4 weeks. Briefly, after general anesthesia of the mice with isoflurane (4%, 400 ml/min, Abbot, AbbVieLtd., United Kingdom), an incision was made on the back of the mouse to create a cavity. The osmotic minipump was placed into the cavity, and the incision was sutured. Body weight was measured at day 0 (before implanting the osmotic minipump), day 1, and 1, 2, 3, and 4 weekends after the implantation of the minipumps. The daily physiological state of the mice was determined. Once a mouse died, an autopsy was performed to determine the cause of death.

2.3 Ultrasonic inspection and measurement

The diameter of the abdominal aorta and cardiac function were measured using the Visual Sonics Vevo 770 (Visual Sonics, Toronto, Canada) ultrasound imaging system, before the mice were sacrificed. B-mode imaging was performed to measure the diameter of the abdominal aorta while M-mode imaging was performed to measure cardiac function. To ensure reproducibility and accuracy of the experiment, all operations were performed by the professional operator who was blinded to the grouping beforehand.

2.4 Collection of tissue samples and serum

The mice were anesthetized with isoflurane (4%, 400 ml/min), and the chest was cut open. The hearts of the mice were exposed, and blood was drawn from the ventriculus dexter. Thereafter, 10–15 ml of normal saline was injected into the ventriculus sinister to flush the residual blood in the aorta. The suprarenal abdominal aorta segment was separated under a stereoscopic microscope and placed into a tissue preservation fluid (Shbio, Shanghai, China) for cell digestion and sc-RNA seq analysis (n = 8 in each group). The extracted blood was placed in coagulation tubes at 20°C for 2 h and then centrifuged at 3000 rpm for 10 min. The supernatant was collected to obtain the serum for subsequent biochemical index determination. Additionally, the abdominal aorta tissue of mice from each group (n=4) was fixed with 5% paraformaldehyde for immunohistochemical (IHC) and immunofluorescence (IF) staining.

2.5 IHC, IF and special stain

The fixed abdominal aorta tissues were embedded in paraffin and cut into 2-μm-thick serial sections for IHC staining. The dyeing steps were as follows: 1) dewaxing and hydration: the sections were incubated in xylene for 10 min at 60°C (twice), the sections were then placed in absolute ethyl alcohol for 5 min (twice), followed by placement in 95% alcohol, 80% alcohol, and 70% alcohol for 2 min each, and finally, the sections were washed with distilled water (three times). 2) Epitope retrieval: The sections were immersed in 0.01 M sodium citrate buffer solution, heated to boil, and then heated for 6 min (four times). 3) Block endogenous catalase activity: The sections were immersed in 3% H_2O_2 for 15 min and then washed with distilled water (three times). 4) Antibody hybrid: After blocking with 20 μl 5% fetal bovine serum (FBS) in phosphate-buffered saline (PBS) at 20°C for 10 min, the sections were incubated in primary antibodies against cluster of differentiation 68 [CD68 (ab955, Abcam, UK, 1:100)], monocyte chemoattractant protein 1 [MCP-1 (ab25124, Abcam, 1:200)], tumor necrosis factor alpha [TNF-α (AF7014, Affinity Biosciences, USA, 1:50)], interleukin 1 beta [IL-1β (26048-1-AP, Proteintech, USA, 1:50)], matrix metallopeptidase 2 [MMP2 (AF0577, Affinity Biosciences, 1:50)], and MMP9 (AF5228, Affinity Biosciences, 1:50) at 4°C overnight. After washing with PBS four times, the sections were incubated with biotin-coupled secondary antibodies at 37°C for 30 min. 5) Coloration: sections were incubated with horseradish peroxidase (HRP) for 20 min at room temperature. After washing with PBS three times, the sections were stained with 0.05% diaminobenzidine (DAB) for 5 min. The sections were then washed with PBS for 3 min (3 times). 6) Counterstaining: The sections were stained with hematoxylin solution for 5 s and washed with PBS until the water was not discolored. 7) Dehydration, clearing, and sealing: The sections were successively incubated with 50% alcohol, 70% alcohol, 95% alcohol, and absolute ethyl alcohol (twice) for 1.5 min each. After incubation with xylene for 1 min (twice), the sections were sealed with a moderate amount of neutral gum.

The dyeing steps of IF were slightly different with IHC and as follow: After epitope retrieval, the sections were incubated with 20 μl 5% FBS in PBS at 20°C for 30 min. Then the sections were co-incubated with primary antibody against vimentin [Vim, (60330-1-Ig, Proteintech, 1:50)] and one of the follow antibody: Cd74 (NB100-1985SS, NOVUS, China, 1:100), fibronectin [Fn1, (15613-1-AP, Proteintech, 1:50)], fibulin-1

[Fbln1, (CL0337, NOVUS, 1:100)], or desmin [Des, (67793-1-Ig, Proteintech, 1:200)] simultaneously at 4°C overnight. After washing with PBS for 3 times, the sections were incubated with fluorescein isothiocyanate (FITC) or tetraethyl rhodamine isothiocyanate (TRITC) conjugated secondary antibody for 30 min at 20°C. After washing with PBS for 2 twice, Diamidinyl phenyl indole (DAPI) was added and incubated for 5 min at 4°C. Finally the sections were washed with PBST for 2 twice and observed with (LSM 900, ZEISS, Germany).

The steps of hematoxylin-eosin (HE), Masson, and Verhoeffs Van Giesof (EVG) dyeing were similar to the steps mentioned above and were adjusted according to the manufacturers' instructions. The degree of degradation of elastic fibers was defined based on previous studies: 1 <25%, 2 ≤25%–≤50%, 3 <50%–≤75%, and 4 >75% [11].

2.6 Single cell preparation and RNA sequencing

The abdominal aorta tissue of the mice was washed with 4°C normal saline solution containing 3% FBS (Thermo Fisher Scientific, Inc.) to remove attached blood clots. The tissue was cut into pieces as small as possible and dissociated into individual cells according to the protocol of the 10× Genomics platform and previous research [11, 16]. Thereafter, arterial tissue fragments were incubated in a specific enzyme solution containing 125 U/ml collagenase type XI (C7657, Sigma, USA), 450 U/ml collagenase type I (C0130, Sigma), 60 U/ml hyaluronidase type I-S (H3506, Sigma), and 60 U/ml DNase I (DNASE10, Sigma) for 1 h at 37°C. The cell suspension was washed twice with normal saline containing 3% FBS, and cell debris was removed through a 70 μl filter. We used a chemiluminescent immunoassay to detect the cell activity. The cells were subjected to sc-RNA seq only when the activity was greater than 85%. Finally, the cell concentration was adjusted to 700/μl.

The whole workflow of sc-RNA seq was based on the protocols of Standard 10x Chromium Single Cell 3' Solution v2 System (10X Genomics Gemcode Technology). The prepared single-cell suspension, 10×barcode gel magnetic beads, and oil droplets were added to different channels of chromium chip B, and the gel beads-in-emulsions (GEMs) were formed through the microfluidic cross-flow system. Each GEM acted as a separate reaction system. The GEMs flowed into the reservoir and were collected. The gel beads were dissolved to release the barcode sequence, which was reverse-transcribed to the cDNA fragment, after which the sample was tagged. After the liquid reservoir was destroyed, PCR amplification was performed using cDNA as a template. All GEM products were mixed to build a standard sequencing library. The double-ended sequencing mode of the Illumina sequencing platform was used to carry out high-throughput sequencing of the constructed libraries.

2.7 Sequencing data processing and analysis

The 10× Genomics Cell Ranger software was used to perform data quality statistical tests on the original data and compare with the reference genomes. Read-matched genomes were divided into exons, introns, and intergenic regions (at least 50% of the bases were matched to exons, introns, and intergenic regions), and when reads were simultaneously matched to an exon and other non-exons, these reads were classified as exon reads in priority. We further analyzed the exon reads combined with the annotation.

The reads were considered to be transcriptome reads when matched to the exon of the transcriptome and when bases were arranged in the same direction. If transcriptome reads were mapped to only one gene, they were unique-mapped, and only unique-mapped reads were used for unique molecular identifier (UMI) counting.

Further cell filtration, standardization, cell subpopulation classification, differentially expressed gene (DEP) analysis of each subpopulation, and marker gene screening were performed using the R package of Seurat v3.0. We filtered the cells based on the number of genes expressed. The specific screening criteria for high-quality cells were as follows: 1) The number of genes identified in a single cell was at least 500; 2) the proportion of mitochondrial gene expression in single cells was less than 25%; 3) Multicellularity was removed using the DoubleFinder package. Data were then log-normalized for subsequent analyses by normalization.

The classification and analysis process of cell subpopulations was as follows: 1) After dimensionality reduction, principal component analysis (PCA) was used to process the normalized expression values. The first ten principal components were selected from the PCA analysis results for subsequent clustering and clustering analysis. 2) The significant principal components were used to construct the k-nearest neighbor clustering diagram based on Euclidean distance. 3) The Jaccard similarity coefficient was used to optimize the weight value of the intercellular distance. 4) A clustering algorithm based on the shared nearest neighbor module optimization was used to identify the cell clusters.

DEPs in different cell clusters were analyzed using the bimod likelihood ratio statistical test to screen for upregulated genes in different cell populations. The screening criteria for upregulated genes were as follows: 1) The genes were expressed in more than 10% of the AAA or CTR subpopulations; 2) a P-value ≤ 0.01; 3) a fold change of upregulated genes ≥ 1.5.

2.8 Gene ontology and Kyoto Encyclopedia of Genes and Genomes analyses

In organisms, different genes coordinate their biological functions with each other. Pathway-based analysis is helpful for further understanding the biological functions of genes. Functional enrichment analysis was performed using the gene ontology (GO) and Kyoto Encyclopedia of Genes and Genomes (KEGG) software online (https://david.ncifcrf.gov/home.jsp). The gene names of the DEGs were listed in an Excel table and uploaded to the online software. The analysis was carried out according to the website's instructions. Enrichment analysis was predominantly used to determine the enrichment degree of differential genes in the GO terms. Hypergeometric tests were used to evaluate the significance of GO terms. The identified pathways that were significantly enriched in DEPs were compared to the entire genome. Statistical differences were considered to be significant when P-value ≤ 0.05.

2.9 Inference of fibroblast state using trajectory analysis

Pseudotime trajectory analysis of single-cell transcriptomes was conducted using Monocle 2. The subsequent analysis steps refer to the process of the official website (http://cole-trapnell-

lab.github.io/monocle-release/docs/#getting-started-with-monocle). We first stored data in a CellDataSet object. The ordering workflow for constructing a single cell trajectory was as follows: 1) Choose the genes that defined progress; 2) reduce dimensions; 3) pseudotime analysis: UMIs were modeled with the negative binomial. Genes that determined the fate of differentiation were selected and processed by metascape software online (https://metascape.org/gp/index.html#/main/step1) to firther reveal biological functions.

2.10 Analysis of intercellular interactions between different cell types

In the following analysis, we used ligand–receptor interactions to evaluate the interactions between different cell types according to the CellPhoneDB database (https://www.cellphonedb.org/documentation). The strength of ligand–receptor interaction between cell types (the interaction score) was defined as the product of the average expression of ligands in cell type A and the average expression of receptors in cell type B. Additionally, we constructed the background distribution of interaction scores based on the idea of perturbation and obtained P-values according to the real interaction scores. Ligand–receptor pairs with P values ≤ 0.05 were selected as targets.

2.11 Statistical analysis

Data analysis and figures making were performed by using GraphPad Prism software (version 5.0; GraphPad Software, San Diego, CA, USA). When the data conformed to normal distribution and homogeneity of variance, Student's t test was used to evaluate the statistical significance, and the results were presented as mean ± standard deviation. Alternatively, Kruskal-Wallis tests were performed on non-normally distributed counting variables. These results were presented as median (quarterback spacing). The Kaplan-Meier test was used to evaluate the difference in survival rate. The relative positive area was calculated by Image J. Differences were considered statistically significant at P ≤ 0.05. The whole workflow was shown in supplement figure.1.

3. Result

3.1 Construction of AAA models and associated physiopathologic characteristics

The weights of all mice were dynamically monitored for 4 weeks after the implantation of minipumps. There was no difference in body weight between the two groups with an increase in feeding time (Supplementary Fig. 2A). One mouse died of AAA rupture on day 26 in the AAA group, while all other mice survived. There was no significant difference in the survival rate between the two groups (P = 0.373, Supplementary Fig. 2B). No significant differences were found in creatine kinase (CK), creatine kinase MB (CKMB), lactic dehydrogenase (LDH), high-density lipoprotein (HDL), low-density lipoprotein (LDL), and

total cholesterol (TC) between the two groups. Interestingly, the levels of blood glucose (GLU) and total triglyceride (TG) were lower in the AAA group, which may be due to a reduction in food intake (Supplementary Fig. 2C).

Ultrasound examination revealed that the intraluminal diameter and intima thickness of the AAA group tended to increase not accompanied by alternation of cardiac function after continuous pumping of Ang II for 28 days (Fig. 1A-1C, Table.1). HE staining results revealed that the basic structure of the artery had been destroyed, and inflammatory cell infiltration was mainly located in the adventitia and media of the artery wall in the AAA group. Masson staining results revealed that SMCs showed a disorderly arrangement accompanied by secondary collagen hyperplasia in the AAA group. EVG staining revealed that the break of elastin layer in the AAA group. Small new elastic fibers were observed in the crevasse (Fig. 1D). Semi-quantitative analysis indicated that there was a tendency for elastin degradation to increase (Fig. 1E). The expression of CD68 and MCP-1 increased in the AAA group, which revealed infiltration of macrophages/monocytes in the arterial wall tissue. Moreover, the expression of cytokines, including TNF-α and IL-1β, increased in the arterial wall tissue (Fig. 1F-J). Additionally, the expression of MMP-2 and MMP-9 increased in the AAA group as was expected (Fig. 1K-M).

3.2 Single cell sequencing identified a total of 25 cell clusters representing eight types of cells

The overall quality parameters of the sc-RNA sequencing data were as follows: A total of 13,779 and 14,086 cells were obtained in the CTR and AAA groups, respectively. The median number of genes per cell was 2734 and 1818 in the CTR and AAA groups, respectively (Supplementary Fig. 3A). Cell activity was an important factor that affected the results. After the removal of low-activity and dead cells, the distribution of the number of genes detected (nFeature_RNA), the total quantity distribution of UMI detected (nCount_RNA), and the percentage of mitochondrial gene expression (Percent.mito) in single cells were obtained (Supplementary Fig. 3B). Cells with mRNA >500 and a proportion of <25% of mitochondrial genes met the standard and were used for subsequent data analysis.

The non-linear dimensionality reduction method of t-distributed stochastic neighbor embedding (t-SNE) was used to visualize the cell subpopulation classification results. A total of 25 cell clusters were isolated from the AAA and CTR groups. In the development of AAA, the cell types, the number of clusters, and the proportion of cells in each group were altered (Fig. 2A).

Different types of cells have specific marker genes. Each type of cell was identified by marker genes [11, 17] and a heatmap indicated that each type of cell was reasonably and distinctly divided (Fig. 2B). A total of eight groups of different cell types were identified (Fig. 2C). The main cell types included: 1) fibroblasts (Fbs) [markers: collagen type III alpha 1 chain (*Col3a1*), collagen type I alpha 1 (*Col1a1*), decorin (*Dcn*), gelsolin (*Gsn*); clusters 0, 1, 2, 6, 7, 12, 15, 22, 23, 24]; 2) monocyte/macrophages (Mo/Møs) [markers: *Cd68*, allograft inflammatory factor 1 (*Aif1*), complement component 1, q subcomponent, beta polypeptide (*C1qb*); clusters 5, 8, 16, 18, 19, 20]; 3) ECs [markers: cadherin 5 (*Cdh5*), platelet/endothelial cell adhesion molecule 1 (*Pecam1*), fatty acid-binding protein 4 (*Fabp4*); clusters 4, 9, 11]; 4) SMCs

[markers: myosin, heavy polypeptide 11 (*Myh11*), actin, alpha 2, smooth muscle, aorta (*Acta2*), transgelin (*Tagln*); clusters 3, 10]; 5) T leukomonocytes (markers: *Cd3d*, *Cd3g*, *Cd28*; cluster 13); 6) B leukomonocytes (markers: *Cd79a*, *Cd79b*, *Cd28*; cluster 21); 7) dendritic cells (DCs) [markers: *Cd209a*, *Cd74*, interferon-induced transmembrane protein 1 (*Ifitm1*); cluster 14]; 8) granulocytes (Gra) [markers: S100 calcium-binding protein A8 (*S100a8*), C-C motif chemokine receptor 1 (*Ccr1*), lymphocyte antigen 6 complex, locus G (*Ly6g*); cluster 17]. The visualization of marker genes confirmed that the markers we selected covered virtually all cells (Fig. 2D) and showed a high degree of differentiation (Fig. 2E). During the formation of AAA, the number of different types of cells in the artery wall tissue was altered: the cell numbers of clusters 1, 2, 3, 5, 8, 9, 10, 12, 17, 18, and 22 increased, while those of clusters 0, 4, 6, 7, 11, 13, 16, 19, 20, 21, 23, and 24 decreased. The cell numbers of clusters 14 and 15 were almost unchanged (Fig. 2F). As for the composition of cells, Fbs and ECs accounted for the largest proportion of artery wall tissue, followed by Mo/Møs and T cells, with B cells, DCs, SMCs, and Gras occupying the smallest proportion in the CTR group. While Fbs and Mo/Møs accounted for the largest proportion of artery wall tissue, followed by SMCs and ECs, and T cells, B cells, DCs, and Gras occupied the smallest proportion in the AAA group (Fig. 2G).

3.3 Immune cells differentiate to promote inflammation during the development of AAA

The transformation of immune cells in the formation of AAA deserves priority attention. Mo/Møs comprised the majority of the immune cells. The proportions of Mo/Mø1, Mo/Mø2, and Mo/Mø4 increased, whereas that of Mo/Mø3, Mo/Mø5, and Mo/Mø6 decreased (Fig. 3A). We selected several M1 marker genes [*Cd86*, *Il1b*, toll like receptor 2 (*Tlr2*), class II major histocompatibility complex transactivator (*Ciita*)] and M2 marker genes [arginase 1 (*Arg1*), *Cd163*, stabilin 1 (*Stab1*), and mannose receptor C-type 1 (*Mrc1*)] to infer the phenotypic transition of macrophages during AAA formation. The t-SNE feature indicated that M2 marker genes, including *Cd163* and *Mrc1*, were mainly expressed in the CTR group. *Stab1* was highly expressed in both groups, whereas *Arg1* was barely expressed in either group. M1 marker genes were irregularly expressed in both the AAA and CTR groups (Fig. 3B-C). The violin plots further indicated that the expression of M1 marker genes in each cluster seemed to be irregular, while M2 marker genes were highly expressed in Mo/Mø3, 5, and 6 (Fig. 3D). The results suggested that the number of M2-type macrophages gradually decreased and that macrophages were polarized in a direction that promoted inflammation as the disease progressed. Type M2 macrophages could be further divided into three subgroups (namely M2a, M2b, and M2c) based on the expression of marker genes [18]. In our study, M2b was rarely expressed in the arterial tissue. M2a was expressed in all CTR clusters (Mo/Mø3, Mo/Mø5, and Mo/Mø6). M2c was predominantly expressed in Mo/Mø5. M2a and M2c macrophages comprised the primary proportion of macrophages in the CTR group and decreased as AAA progressed (Fig. 3E-F).

T and B cells are important components of the immune cells. In this experiment, fewer T and B cells were identified in the AAA group (Fig. 3A). During the development of AAA, the expression of *Cd3* and *Cd8* increased significantly, while *Cd4* expression was similar in both groups (Fig. 3G). Bioinformatic analysis

further revealed the functional alternations of T lymphocytes. Ribosome-related components, translation, T cell differentiation and activation, protein binding, and the structural constituent of ribosomes accounted for the majority of the GO enrichment terms. During the formation of AAA, the protein synthesis of T lymphocytes increased, and the differentiation and activation of cells was vibrant (Supplementary Fig. 4A). KEGG pathway analysis suggested that protein synthesis (ribosome) and T cell activation and differentiation were the most critical mechanism alterations (Supplementary Fig. 4B).

After activation, B lymphocytes can differentiate into plasma cells. In addition to synthesizing and secreting various immunoglobulins, plasma cells also highly express *Cd38* and *Cd27*, while there is a low expression of *Cd5*, which is consistent with the current results (Fig. 3H). Further bioinformatic analysis suggested that ribosome-related components, immune system process, translation, cytoplasmic translation, mRNA processing, and protein binding accounted for the majority of the GO enrichment terms (Supplementary Fig. 4C). KEGG pathway analysis suggested that the B cell receptor signaling pathway, protein synthesis (ribosome) pathway, and NF-κB signaling pathway were critical pathways in the AAA process. Additionally, the activation of B cells also affected the differentiation and function of T lymphocytes (Supplementary Fig. 4D).

3.4 Transformation in the function and phenotype of SMCs and ECs during the formation of AAA

SMCs and ECs are important components of the artery wall tissue. Corresponding functional and phenotypic changes in SMCs and ECs also occurred during the disease process of AAA. The numbers of EC1 and EC3 generally decreased, while that of EC2 increased during AAA formation, and numbers of both SMC1 and SMC2 increased (Fig. 4A). The top 10 marker genes of ECs were identified for each cluster relative to all other clusters. The expression patterns of marker genes in EC1 and EC3 were similar, which was different from that of EC2 (Fig. 4B). Phlogosis and damage-related genes, including vascular cell adhesion molecule-1 (*Vcam1*), von Willebrand factor (*Vwf*), intercellular adhesion molecule 1 (*Icam1*), endothelin 1 (*Edn1*), *Serpine1*, and prostaglandin I2 synthase (*Ptgis*) [19–22], were highly expressed in EC2. Proliferation and regeneration-related genes, including endoglin (*Eng*), kinase insert domain receptor (*Kdr*), and chromodomain helicase DNA-binding protein 5 (*Chd5*) [23–25], were highly expressed in EC1 and 3 (Fig. 4C), which was further confirmed by the violin plot (Fig. 4D).

Similar phenotypic and functional changes were observed in the SMC. The expression of secretory SMC marker genes [secreted phosphoprotein 1 (*Spp1*), matrix Gla protein (*Mgp*), epiregulin (*Ereg*), and elastin (*Eln*)] increased in SMC1 and SMC2, while the expression of contractile SMC marker genes [*Acta2*, *Tagln*, caldesmon 1 (*Cald1*), and *Myh11*] remained unchanged during AAA formation (Fig. 4E), which implied a transition of SMCs from contractile to secretory during the formation of AAA.

3.5 The cell heterogeneity and DEG expression of Fbs in AAA

Fibroblasts were identified into most clusters in our study. During the AAA process, the amount of Fb1, Fb4, Fb5, Fb9, and Fb10 decreased while Fb2, Fb3, Fb6, and Fb8 increased, Fb7 was basically unchanged (Fig. 5A). The top 10 marker genes were identified for each cluster relative to all the other clusters. Clusters with the same trends in amount had similar gene expression mode (Fig. 5B). Further screening of DEGs was necessary. A total of 411 upregulated genes and 605 downregulated genes were identified (Fig. 5C). GO enrichment analysis revealed that Fbs were predominantly involved in the binding of collagen and the synthesis and degradation of ECM (Fig. 5D). KEGG pathway analysis revealed that oxidative phosphorylation, ECM-receptor interaction, and PI3K-Akt signaling pathway may be the pivotal signaling pathways that participate in the formation of AAA (Fig. 5E).

3.6 Single cell trajectory analysis predicted cell differentiation of Fbs in AAA

The process of phenotypic and functional alternations in the cells was gradual. Therefore, it was not clear which pattern of Fbs was responsible for AAA initiation. The pseudo-time of Fbs with gene expression profiles of different clusters was reconstituted (Fig. 6A). Gene expression could be roughly divided into seven stages according to the different nodes (Fig. 6B). The typical direction of Fb differentiation was the transformation from stage 1 to stage 4. The t-SNE map also reflected the direction of cell differentiation; dark-colored cells continued to transform into light-colored cells (Fig. 6C). We identified that Fb5 was the starting point of differentiation and ultimately differentiated into Fb2 and Fb6. The heatmap displays the alternation tendencies of the top 50 critical genes. Overall, we found three different patterns of genetic changes, namely, Cluster 1: The expression of genes first increased and then decreased with the development of AAA, including that of ribosomal protein L37a (*Rpl37a*), ribosomal protein S20 (*Rps20*), and ribosomal protein S27 (*Rps27*); Cluster 2: The expression of genes decreased with the development of AAA, including that of myelin and lymphocyte protein, T cell differentiation protein (*Mal*) and noncompact myelin-associated protein (*Ncmap*); Cluster 3: The expression of genes increased with the development of AAA, including that of complement component factor h (*Cfh*), biglycan (*Bgn*), and v-maf musculoaponeurotic fibrosarcoma oncogene family, protein B (*Mafb*) (Fig. 6D). The top six genes displaying the most distinct expression change were considered to have determined the outcome of Fb differentiation. The relative expression levels of the top six genes were shown over pseudotime by Monocle2 in cluster mode (Fig. 6E) and state mode (Fig. 6F).

As we selected the top 50 genes which determined the direction of Fbs differentiation, further bioinformatics studies were necessary. The overlap of the 3 clusters was shown in the circus plot and the blue curves link genes that belong to the same enriched ontology term (Fig. 6G). The heatmap of GO enrichment terms shown that genes listed in cluster 3 (up expressed) mainly participated in negative regulation of immune system process, regulation of complement cascade and antigen processing and present; genes in cluster 2 (down expressed) mainly participated in myelination; genes in cluster 1 (first up and then down expressed) mainly participated in SRP-dependent cotranslational protein targeting to membrane, negative regulation of peptidase activity, post-translational protein phosphorylation, platelet degranulation, protein localization to membrane, response to endoplasmic reticulum stress, vesicle

organization and response to metal ion (Fig. 6H). To further capture the relationships between the terms, a subset of enriched terms had been selected and rendered as a network plot (Fig. 6I). Although no common GO enrichment terms were found between the 3 clusters, it seemed that cluster 1 was associated with cluster 3 according part of the GO terms, which involved in regulation of the immune system, phosphorylation of post-translational protein and degranulation of platelets.

3.7 Analysis of marker genes revealed different subtypes of increased fibroblasts in function and spatial distribution

It was necessary to identify Fbs through the expression of specific markers. Seven different terms were identified, namely, normal quiescent state [*Vim* and caveolin 1 (*Cav1*)] [26], active state [*S100a8*, fibroblast activation protein alpha (*Fap*), *Acta2*, platelet-derived growth factor receptor beta (*Pdgfrb*)] [27, 28], antigen presentation [*Cd74* and histocompatibility 2, class II antigen A, beta 1 (*H2-Ab1*)] [29], phlogosis (*Il1b* and *Il6*) [30], angiogenesis (*Des*) [31], extracellular matrix synthesis [platelet-derived growth factor receptor alpha (*Pdgfra*) and fibulin 1 (*Fbln1*)] [32] and tissue repair [fibronectin 1 (*Fn1*)] [33]. The dot plot showed the expression of characteristic genes in different Fb clusters (Fig. 7A). Based on the results from single-cell trajectory analysis, Fb5 might be the starting point of differentiation (Fig. 6C) and was selected as the control cluster. Semi-quantitative analysis showed the difference in the expression of related functional genes between Fb5 and increased Fbs in the expression of related functional genes (Fig. 7B). The expression of marker genes in increased Fbs was compared with that of Fb5, and the values of fold change (FC) were obtained. The increased Fbs were redefined according to the FC values (Fig. 7C). The criteria were as follows: 0 (0.5<FC value<2); + (2≤FC value<4); ++ (4≤FC value<8); +++ (8≤FC value); - (0.25<FC value≤0.5); – (0.125<FC value≤0.25); — (FC value≤0.125). Fb2 highly expressed *Cd74* and *H2-Ab1* and was defined as an antigen presenting Fb (apFb). Fb6 highly expressed in *Fn1* and was defined as tissue repair Fb (trFb). Fb8 highly expressed Des and was defined as vascular Fb (vFb). Fb3 only highly expressed in activation-related markers and was defined as activation Fb (acFb). Immunofluorescence confirmed the presence of 4 Fbs in AAA tissue (Fig. 7D), Fb2 co-expressed *Vim* and *Cd74* and can be observed in the whole artery layer of AAA tissue; Fb3 highly co-expressed Fbln1 and Vim, and mainly distributed in the intima of arteries; Fb6 highly co-expressed Fn1 and Vim, which was mainly observed around thrombus; Fb8 high co-expressed *Des* and *Vim*. As the smallest subgroup, it was hardly been discovered for its small amount.

3.8 The ligand–receptor interaction analysis revealed the procollagen synthesis effect of Fbs on SMCs

Cell-cell communication was investigated by ligand–receptor analysis according to CellPhoneDB. The results indicated that the intensity of the interaction between different types of cells varied greatly. Meanwhile, the Fbs had the closest connection with the SMCs (Fig. 8A). We further processed the ligand–receptor analysis between SMCs and increased Fbs (Fb2, Fb3, Fb6, and Fb8) during AAA formation. Fb3 and Fb6 were found to have more connections with SMCs than Fb2 and Fb8 (Fig. 8B). Four distinct Fb clusters influenced the function and phenotype of SMC through multiple ligand–receptor pairs (Fig. 8C-

F). Different Fb/SMC pairs showed specific ligand–receptor characteristics. We found that *CD74*-macrophage migration inhibitory factor (*Mif*), *Cd74*- COPI coat complex subunit alpha (*Copa*), and *CD74*-amyloid beta precursor protein (*App*) displayed important associations between Fb2 and SMCs, confirming the antigen-presenting effect of Fb2. The *Fn1–a5b1 complex*, *Fbn1–a5b1 complex*, *Fn1–a8b1 complex*, *Fn1–aVb1 complex*, and *Fn1–aVb5 complex* were critical links between Fb6 and SMC, which demonstrated that Fb6 played an important role in tissue repair during disease progression. Alternatively, increased collagen synthesis was the most prominent feature of the selected Fbs, except Fb8. Additionally, the expression of *Spp1- a9b1 complex* and fibroblast growth factor receptors (*Fgfr1*)-neural cell adhesion molecule 1 (*Ncam1*) commonly increased significantly while neuropilin-1 (*Nrp1*)-vascular endothelial growth factor B (*Vegfb*) and *Pdgfr* complex- platelet-derived growth factor D (*Pdgfd*) were decreased in 4 Fbs.

4. Discussion

The occurrence of vascular-associated diseases is often accompanied by the functional and phenotypic transformation of different types of cells. Sc-RNA seq provides critical support for elucidating the mechanism of disease by indicating cellular heterogeneity. In this experiment, we processed sc-RNA seq data of >20,000 individual cells from the abdominal aorta tissue of the upper renal artery that was exposed to either Ang II or to normal saline. Finally, 25 clusters and eight different cell lines were identified. Based on the marker genes expressed in each cell cluster, we explained the transformations in cellular function and phenotype in Ang II-induced AAA. Further bioinformatics analysis of DEGs and differentiation trajectory revealed that Fb played an important role in the synthesis and degradation of ECM and the regulation of immune system. Finally, the ligand-receptor analysis between increased Fbs and SMCs was performed and found that increased collagen synthesis was an important feature of Ang II-induced AAA. Overall, our experiment mapped the cellular heterogeneity of Ang II-induced AAA. Fibroblasts transformed into different phenotypes during the course of disease and participated in regulation of immune system and the metabolic homeostasis in ECM. Its heterogeneity played a critical role in pathophysiological process of Ang II-induced AAA.

Comparisons with previous studies would help us better understand our results. Hadi et al. also investigated the cellular heterogeneity of arterial tissue in Ang II-induced AAA. They found that Fbs made up the largest population in the tissue of AAA which was consisted with our results[34]. It suggested that Fb may play a critical role in the pathophysiological process of Ang II-induced AAA, however the potential pathogenic mechanism had not been elucidated in Hadi's research. In the other hand, Zhao et al. found that macrophages were the largest population, and immune cells accounted for more than 60% of the total number of cells in elastase-induced AAA group. Additionally, natural killer cells, erythrocytes, and neurocytes were exclusive cell types in elastase-induced AAA models, whereas granulocytes were only found in Ang II-induced AAA[11]. The reasons for these differences may predominantly be the unequal levels of predisposing factors present within the two models.

The amount of macrophages occupied an absolutely important position in immune cells. In fact, most macrophages in the aorta were derived from circulating monocytes [35]. After colonization in tissues, macrophages perform a variety of functions, including secretion of proinflammatory factors and MMPs, activating oxidative stress response, and participating in thrombosis and vascular remodeling [36]. Our research found that the expression of M2 macrophage marker genes (mainly in Mo/Mø3, Mo/Mø5, and Mo/Mø6) decreased while M1-type macrophage marker genes, however, did not appear to increase as the AAA progressed. Previous studies had confirmed that Ang II induces the differentiation of macrophages into M1 type in AAA [37, 38]. We speculated that the process of mRNA translation into polypeptides was regulated by small molecules, such as miRNA, which resulted in the increased synthesis of the marker protein. Alternations in the microenvironment were crucial for macrophage polarization, as studies have confirmed that M1-like phenotype macrophages can dedifferentiate and switch to M2-like macrophages when the microenvironment was altered [39]. M2-type macrophages play an immunoregulatory role in the formation of AAA and our results confirmed that M2a and M2c were the main M2-type macrophages in the arterial tissue, which was not been reported before. Different subtypes of M2-type macrophages played their respective physiological roles, and its role in the AAA process deserved greater attention.

Despite the small amount of identified T and B cells, critical phenotypic and functional changes occurred during the formation of AAA. The expression of CD3 in T lymphocytes improved in the AAA group. CD3 binds tightly to T-cell receptor to form a multisubunit complex and further induces phosphorylation of immunoreceptor tyrosine-based activation motifs, which triggers a T-cell effector response, resulting in the activation of T cells [40]. Both $CD8^+$ and $CD4^+$ lymphocytes have been confirmed to involved in vascular inflammation in AAA [41, 42]. Our results showed that the expression of CD8 increased, while CD4 expression barely changed during the AAA process. In addition, we found that plasma cells increased in arterial tissue during AAA formation, which was confirmed by previous studies [43]. Overall, inflammatory cells tend to differentiate in a proinflammatory direction during the process of AAA.

The heterogeneity of non-immune cells is also worthy of attention. We found that the amount of EC1 and EC3, with high expression of proliferation and regeneration-related genes, decreased, while EC2 showed a high expression of inflammation and damage-related genes during the disease process in our results. The ability of ECs to produce nitric oxide (NO) is critical to adapt microenvironmental alterations. ECs contribute to the AAA process predominantly through oxidative stress mediation by impairing NO bioavailability [44, 45], suggesting that dysfunction of ECs is an important characteristic of AAA. Similar functional transformations were also observed in SMC. We identified two clusters of SMCs in total, both of which increased during AAA formation. The number of SMCs captured in this experiment was insufficient to conclude SMCs as the most important cell ingredient in normal artery tissue. These discrepancies were likely associated with technical aspects, including the enzymatic cocktails used for single-cell release and the different approaches to data analysis[11]. With regards to cell function, we found that the expression of contractile phenotype-related genes remained largely unchanged, while the expression of secretory phenotype-related genes increased simultaneously. The literature suggests that vascular SMCs play a variety of roles in the progression of AAA. They mediate the production and

degradation of ECM, transdifferentiate into macrophage-like cells, mediate inflammation, upregulate the levels of cytokines, and downregulate the expression of antioxidant genes which was consisted with our results [46]. Limited by the small number of identified SMCs, we only performed a simple analysis. Analysis with a larger size sample was necessary.

Fbs were the most specific cell type identified; not only their number occupied an absolute advantage in the total cells, but also their extensive cellular heterogeneity and functional differences. Previous studies have confirmed that Fbs play numerous pathophysiological roles in blood vessel wall tissues, including in angiogenesis, vascular inflammation, and promoting the migration of ECs [47, 48]. Analysis of DEGs provided us with a understanding of the changes in Fb function. The expression of *Acta2, Tagln*, and *Spp1* increased, suggesting that Fbs gradually differentiated into myofibroblasts during AAA formation. A study performed by Sakata demonstrated that myofibroblasts participated in the vascular remodeling of inflammatory aortic aneurysm (IAA) by inducing the production of hypoxia-inducible factor 1 [49]. Cellular communication network factor 2 (*Ccn2*), also known as connective tissue growth factor (*Ctgf*), is a marker of fibrosis. It has been confirmed that *Ctgf* promotes proliferation, migration, and differentiation of Fbs [50]. Cartilage oligomeric matrix protein (*Comp*) is a component of ECM. Yi Fu et al found that it could act as an endogenous β-arrestin-2-selective allosteric modulator of AT1 receptor counteracting vascular injury. Its deficiency aggravated AngII-induced AAA formation [51]. Thrombospondin-1 (*Thbs1*) also is a matricellular protein involved in the maintenance of vascular structure and homeostasis through the regulation of cell proliferation, apoptosis, and adhesion. Liu Zhenjie et al reported that *Thbs1 -/-* mice were resistant to aneurysm induction [52], which was different with results from another related research [53]. It suggested that the role of *Thbs1* in the formation of AAA was two-sided. Complement factor D (*Cfd*), as a member of the alternative complement pathway, is the rate-limiting enzyme of for the formation of C3 convertase. Although the complement system has been proved to play a critical role in the development of AAA [54, 55], there is no specific study between *Cfd* and AAA. Due to its important role in complement systems (rate-limiting enzyme of C3 convertase), *Cfd* may be a potential target for the treatment of AAA.

Single-cell trajectory analysis provided further insights into the differentiation process of Fbs in AAA process. The top 50 genes that had the most substantial influence on cell transformation were selected and roughly divided into three categories according to their expression. In brief, genes with increased expression mainly played a role in regulation of complement cascade, negative regulation of immune system process and antigen processing and present, which was consistent with the results of our DEG research. Genes with decreased expression predominantly involved in myelination, however no association between it and AAA has been reported so far. Genes with an expression that first increased and then decreased were largely related to SRP-dependent cotranslational protein targeting to membrane and negative regulation of peptidase activity. They participated in translation, peptide metabolic processes, and ribosome assembly. The network plot revealed that immunomodulatory alternations, especially in complement system, are important features of Fb reprogramming during formation of Ang-II induced AAA.

In order to further explore the role of Fb in the AAA process, it was necessary to classify clusters of Fbs in more detail based on their functional marker genes. Previous studies on tumor provided a classification standard of cancer-associated fibroblasts (CAF) which was adopted in our research [29, 31]. The 4 increased Fbs performed various functions and distributed in different areas of aneurysm tissue confirmed by immunofluorescence. Even in elastase-induced mice AAA models, fibroblasts also accounted for a significant proportion, however, its role in AAA process was underappreciate [11]. Our research confirmed that Fbs were not only involved in tissue repair, ECM metabolic homeostasis, but also in immune system regulation in aneurysm tissue. In addition, fibroblasts gradually transform into myofibroblasts which promoted the vascular remodeling under Ang-II stimulation. Interestingly, *Des* and *Cav1* were highly expressed in Fb8, which suggested that Fb8 was an intermediate state cell between Fbs and SMCs. Its role in the occurrence and development of AAA was still undefined and deserved further study.

Further ligand-receptor analysis revealed the expression of molecular signals between 4 increased Fbs and SMCs. Increased collagen synthesis was the main feature of communication between Fbs and SMCs. It had been confirmed that the expression of collagen type I/III cross-links was particularly prominent in human AAA tissue, however, total collagen markers were decreased (decreased 4-hypro and 5-hylys) it was reasonable to suggest that new collagen biosynthesis was somehow defective [56]. In adition, 4 ligand–receptor pairs were common significantly altered in four Fbs. *Spp1-a9b1*, also known as osteopontin (*Opn*), has been confirmed to be involved in the migration of SMCs and vascular remodeling [57, 58]. *Ncam1* is mainly expressed in central nerve cells and can induce neurogenesis and stimulate cell-matrix adhesion and neurite outgrowth by activating *Fgfr* signaling [59], there are few reports of its involvement in cardiovascular disease. *Nrp1-Vegfb* mainly participates in the proliferation of SMCs and is associated with increased vascular diameter [60]. It also promotes the progression of inflammation and the transport of fatty acids in ECs [61]. *Pdgfd* was identified as the critical molecule in promoting vascular smooth muscle remodeling. Associated studies revealed that *Pdgfd* was found to be highly expressed in perivascular adipose tissue (PVAT) in AAA models of leptin-deficient mice. *Pdgfd* may mediate inflammation of the vascular adventitia [62]. Previous studies had confirmed that the above ligand-receptors were involved in promoting vascular remodeling and inflammatory response except *Ncam1-Fgfr*. However the expression of *Nrp1-Vegfb* and *Pdgfd-Pdgfr* decreased in AAA. Whether the phenomena were the secondary changes of AAA still required further research.

In summary, our study revealed the cellular heterogeneity of Ang II-induced AAA in mice, according to sc-RNA sequencing. These findings complement our understanding of the pathophysiological characteristics of AAA. However, there were some limitations in our study. 1) As one of the important components of the vascular media, the amount of captured vascular smooth muscle cells was insufficient. The quality inspection of single-cell RNA sequencing verified that our samples were up to standard. We suspected that discrepancies were likely associated with technical aspects, including the enzymatic cocktails used for single-cell release and the different approaches to data analysis. A larger sample size might eliminate the differences. 2) The aim of this study was to complete the cell map of Ang-II mediated AAA. In-depth analysis of the potential mechanisms and prognostic effects of specific

type of cell on disease were not performed in this research. In the future, we will conduct further mechanism research and functional verification on the interaction between Fbs and smooth muscle cells. 3) In this study we did not measure blood pressure of mice after Ang II pumping. Although previous research reported that Ang II infusion promoted AAA independent of increased blood pressure [63], it reduced the preciseness of our research.

5. Conclusion

In general, our study mapped the cell atlas of Ang II-induced AAA. By using sc-RNA sequencing technology, we revealed the pivotal role of fibroblast heterogeneity in Ang II-induced AAA. It mainly participated in the process of AAA by regulating the immune system and the metabolic balance of ECM. Our study may provide a new perspective on emergence and development of aortic disease under different condition. Future studies should address on clinical efficacy of potential therapeutic targets selected by sc-RNA seq and validation of mechanism.

6. Abbreviation

Abbreviation	Description
AAA	abdominal aortic aneurysm
acFb	activation fibroblast
Acta2	actin, alpha 2, smooth muscle, aorta
ADA	aortic dissection aneurysm
Aif1	allograft inflammatory factor 1
Ang	angiotensin
apFb	antigen presenting fibroblast
Apoe	apolipoprotein E
App	amyloid beta precursor protein
Arg1	arginase 1
Bgn	biglycan
C1qb	complement component 1, q subcomponent, beta polypeptide
$CaCl_2$	calcium chloride
Cald1	caldesmon 1
Cav1	caveolin 1
Ccn2	Cellular communication network factor 2
Ccr1	C-C motif chemokine receptor 1
CD/Cd	cluster of differentiation
Cdh5	cadherin 5
Cfd	Complement factor D
Cfh	complement component factor h
Chd5	chromodomain helicase DNA-binding protein 5
CK	creatine kinase
CKMB	creatine kinase MB
Ciita	class II major histocompatibility complex transactivator
Col1a1	collagen type I alpha 1
Col3a1	collagen type III alpha 1 chain
Comp	Cartilage oligomeric matrix protein

Copa	COPI coat complex subunit alpha
Ctgf	connective tissue growth factor
CTR	control
DAB	diaminobenzidine
DAPI	Diamidinyl phenyl indole
DC	dendritic cell
Dcn	decorin
DEP	differentially expressed gene
Des	desmin
EC	endothelial cell
ECM	extracellular matrix
Edn1	endothelin 1
Eln	elastin
Eng	endoglin
Ereg	epiregulin
EVG	Verhoeffs Van Giesof
Fabp4	fatty acid-binding protein 4
Fap	activation protein alpha
Fbln1	fibulin-1
Fbs	fibroblasts
FBS	fetal bovine serum
Fgfr	fibroblast growth factor receptors
FITC	fluorescein isothiocyanate
Fn	fibronectin
GEM	gel beads-in-emulsion
GLU	glucose
GO	gene ontology
Gra	granulocytes
Gsn	gelsolin

H2-Ab1	histocompatibility 2, class II antigen A, beta 1
HDL	high-density lipoprotein
HE	hematoxylin-eosin
HRP	horseradish peroxidase
IF	immunofluorescence
Ifitm1	interferon-induced transmembrane protein 1
IHC	immunohistochemical
IL-1β/Il-1b	interleukin 1 beta
Icam1	intercellular adhesion molecule 1
Kdr	kinase insert domain receptor
KEGG	Kyoto Encyclopedia of Genes and Genomes
LDH	lactic dehydrogenase
LDL	low-density lipoprotein
Ly6g	lymphocyte antigen 6 complex, locus G
Mafb	v-maf musculoaponeurotic fibrosarcoma oncogene family, protein B
Mal	myelin and lymphocyte protein, T cell differentiation protein
MCP-1	monocyte chemoattractant protein 1
Mgp	matrix Gla protein
Mif	macrophage migration inhibitory factor
MMP	matrix metalloproteinase
Mo/Mø	monocyte/macrophage
Mrc1	mannose receptor C-type 1
Myh11	myosin, heavy polypeptide 11
Ncam1	neural cell adhesion molecule 1
Ncmap	noncompact myelin-associated protein
Nrp1	neuropilin-1
Opn	osteopontin
PBS	phosphate-buffered saline
PCA	principal component analysis

Pdgfd	pdgfr complex- platelet-derived growth factor D
Pdgfr	platelet-derived growth factor receptor
Pecam1	platelet/endothelial cell adhesion molecule 1
PI3K-Akt	phosphatidylinositol 3-kinase-protein kinase B
Ptgis	prostaglandin I2 synthase
PVAT	perivascular adipose tissue
RAAS	renin-angiotensin-aldosterone system
Rpl	ribosomal protein L
Rps	ribosomal protein S
S100a8	S100 calcium-binding protein A8
sc-RNA seq	single-cell RNA sequencing
SMC	smooth muscle cell
SPF	specific pathogen free
Spp1	secreted phosphoprotein 1
Stab1	stabilin 1
Tagln	transgelin
TC	total cholesterol
TG	total triglyceride
Thbs1	Thrombospondin-1
Tlr2	toll like receptor 2
TNF-α	tumor necrosis factor alpha
trFb	tissue repair fibroblast
TRITC	tetraethyl rhodamine isothiocyanate
t-SNE	t-distributed stochastic neighbor embedding
UMI	unique molecular identifier
Vcam1	vascular cell adhesion molecule-1
Vegfb	vascular endothelial growth factor B
vFb	vascular fibroblast
Vim	vimentin

Vwf	von Willebrand factor

Declarations

Declaration of conflicting interest

All authors had no conflicting interest of the work.

Acknowledgements and fundings

The present study was supported by grants obtained from the National Natural Science Foundation of China (grant no. 81770475), the Natural Science Foundation of Zhejiang Province (grant no. LY21H020002). The LC-Bio Technology co.ltd., (Hangzhou, China) provided the technical support and experimental platform of 10x sc-RNA seq.

Authors contributions

Yingzheng Weng analyzed the data and wrote the manuscript. Yingzheng Weng, Changhong Cai and Jiangjie Lou were responsible for AAA modeling, animal rearing and data recording of all mice. Yizong Bao and Changqing Du performed the production of pictures and tables. Kefu Zhu was responsible for the operation of ultrasound. Lijiang Tang and Xiaofeng Chen were responsible for the conception and experimental guidance of the experiment. All authors read and approved the final manuscript.

Ethics approval and consent to participate

All our operations were in line with“Guiding Principles in the Care and Use of Animals” (China). Ethics approval was obtained from laboratory of Zhejiang Academy of Medical Sciences (No. 20200271) prior to the start of the study.

Consent for publication

Not applicable

Availability of data and materia

The datasets used or analysed during the current study are available from the corresponding author on reasonable request.

References

1. Ullery, B.W., R.L. Hallett, and D. Fleischmann, *Epidemiology and contemporary management of abdominal aortic aneurysms.* Abdom Radiol (NY), 2018. **43**(5): p. 1032-1043.
2. Golledge, J., *Abdominal aortic aneurysm: update on pathogenesis and medical treatments.* Nat Rev Cardiol, 2019. **16**(4): p. 225-242.

3. Toghill, B.J., A. Saratzis, and M.J. Bown, *Abdominal aortic aneurysm-an independent disease to atherosclerosis?* Cardiovasc Pathol, 2017. **27**: p. 71-75.
4. Peshkova, I.O., G. Schaefer, and E.K. Koltsova, *Atherosclerosis and aortic aneurysm - is inflammation a common denominator?* Febs j, 2016. **283**(9): p. 1636-52.
5. Climent, E., et al., *Diabetes mellitus as a protective factor of abdominal aortic aneurysm: Possible mechanisms.* Clin Investig Arterioscler, 2018. **30**(4): p. 181-187.
6. Jana, S., M. Hu, and M. Shen, *Extracellular matrix, regional heterogeneity of the aorta, and aortic aneurysm.* 2019. **51**(12): p. 1-15.
7. Moxon, J.V., et al., *Proteomic and genomic analyses suggest the association of apolipoprotein C1 with abdominal aortic aneurysm.* Proteomics Clin Appl, 2014. **8**(9-10): p. 762-72.
8. Gurung, R., et al., *Genetic and Epigenetic Mechanisms Underlying Vascular Smooth Muscle Cell Phenotypic Modulation in Abdominal Aortic Aneurysm.* Int J Mol Sci, 2020. **21**(17).
9. Tedjawirja, V.N. and V. de Waard, *Which Mouse Model of Abdominal Aortic Aneurysm Deserves Triple A Status?* Eur J Vasc Endovasc Surg, 2019. **58**(5): p. 777-778.
10. Xuan, H., et al., *Inhibition or deletion of angiotensin II type 1 receptor suppresses elastase-induced experimental abdominal aortic aneurysms.* J Vasc Surg, 2018. **67**(2): p. 573-584.e2.
11. Zhao, G., et al., *Single-cell RNA sequencing reveals the cellular heterogeneity of aneurysmal infrarenal abdominal aorta.* Cardiovasc Res, 2021. **117**(5): p. 1402-1416.
12. Mulorz, J., et al., *Hyperlipidemia does not affect development of elastase-induced abdominal aortic aneurysm in mice.* Atherosclerosis, 2020. **311**: p. 73-83.
13. Wang, Y., S. Krishna, and J. Golledge, *The calcium chloride-induced rodent model of abdominal aortic aneurysm.* Nat Commun, 2013. **226**(1): p. 29-39.
14. Trachet, B., et al., *Dissecting abdominal aortic aneurysm in Ang II-infused mice: suprarenal branch ruptures and apparent luminal dilatation.* Cardiovasc Res, 2015. **105**(2): p. 213-22.
15. Yang, H., et al., *Single-Cell RNA Sequencing Reveals Heterogeneity of Vascular Cells in Early Stage Murine Abdominal Aortic Aneurysm-Brief Report.* Arterioscler Thromb Vasc Biol, 2021. **41**(3): p. 1158-1166.
16. Kalluri, A.S., et al., *Single-Cell Analysis of the Normal Mouse Aorta Reveals Functionally Distinct Endothelial Cell Populations.* Circulation, 2019. **140**(2): p. 147-163.
17. Li, Y., et al., *Single-Cell Transcriptome Analysis Reveals Dynamic Cell Populations and Differential Gene Expression Patterns in Control and Aneurysmal Human Aortic Tissue.* Circulation, 2020. **142**(14): p. 1374-1388.
18. Martinez, F.O., et al., *Macrophage activation and polarization.* Front Biosci, 2008. **13**: p. 453-61.
19. Wang, X.J., et al., *Association of Rare PTGIS Variants With Susceptibility and Pulmonary Vascular Response in Patients With Idiopathic Pulmonary Arterial Hypertension.* JAMA Cardiol, 2020. **5**(6): p. 677-684.

20. Folco, E.J., et al., *Neutrophil Extracellular Traps Induce Endothelial Cell Activation and Tissue Factor Production Through Interleukin-1α and Cathepsin G.* Arterioscler Thromb Vasc Biol, 2018. **38**(8): p. 1901-1912.
21. Sharda, A.V., et al., *VWF maturation and release are controlled by 2 regulators of Weibel-Palade body biogenesis: exocyst and BLOC-2.* Blood, 2020. **136**(24): p. 2824-2837.
22. Pulido, I., et al., *Endothelin-1-Mediated Drug Resistance in EGFR-Mutant Non-Small Cell Lung Carcinoma.* 2020. **80**(19): p. 4224-4232.
23. Cao, S., et al., *The upregulation of miR-101 promotes vascular endothelial cell apoptosis and suppresses cell migration in acute coronary syndrome by targeting CDH5.* Int J Clin Exp Pathol, 2019. **12**(9): p. 3320-3328.
24. Guerin, C.L., et al., *Multidimensional Proteomic Approach of Endothelial Progenitors Demonstrate Expression of KDR Restricted to CD19 Cells.* 2021. **17**(2): p. 639-651.
25. Lawera, A., et al., *Role of soluble endoglin in BMP9 signaling.* 2019. **116**(36): p. 17800-17808.
26. Rai, A., et al., *Exosomes Derived from Human Primary and Metastatic Colorectal Cancer Cells Contribute to Functional Heterogeneity of Activated Fibroblasts by Reprogramming Their Proteome.* Proteomics, 2019. **19**(8): p. e1800148.
27. Kaps, L. and D. Schuppan, *Targeting Cancer Associated Fibroblasts in Liver Fibrosis and Liver Cancer Using Nanocarriers.* Cells, 2020. **9**(9).
28. Ghosh, D., et al., *Leveraging Multilayered "Omics" Data for Atopic Dermatitis: A Road Map to Precision Medicine.* Front Immunol, 2018. **9**: p. 2727.
29. Elyada, E., et al., *Cross-Species Single-Cell Analysis of Pancreatic Ductal Adenocarcinoma Reveals Antigen-Presenting Cancer-Associated Fibroblasts.* 2019. **9**(8): p. 1102-1123.
30. Öhlund, D., et al., *Distinct populations of inflammatory fibroblasts and myofibroblasts in pancreatic cancer.* 2017. **214**(3): p. 579-596.
31. Bartoschek, M., N. Oskolkov, and M. Bocci, *Spatially and functionally distinct subclasses of breast cancer-associated fibroblasts revealed by single cell RNA sequencing.* 2018. **9**(1): p. 5150.
32. Friedman, G., et al., *Cancer-associated fibroblast compositions change with breast cancer progression linking the ratio of S100A4+ and PDPN+ CAFs to clinical outcome.* Nature Cancer, 2020. **1**(7): p. 1-17.
33. Miron-Mendoza, M., et al., *Fibroblast-fibronectin patterning and network formation in 3D fibrin matrices.* Matrix Biol, 2017. **64**: p. 69-80.
34. Hadi, T., L. Boytard, and M. Silvestro, *Macrophage-derived netrin-1 promotes abdominal aortic aneurysm formation by activating MMP3 in vascular smooth muscle cells.* 2018. **9**(1): p. 5022.
35. Davis, F.M., D.L. Rateri, and A. Daugherty, *Mechanisms of aortic aneurysm formation: translating preclinical studies into clinical therapies.* Heart, 2014. **100**(19): p. 1498-505.
36. Yuan, Z., et al., *Abdominal Aortic Aneurysm: Roles of Inflammatory Cells.* Front Immunol, 2020. **11**: p. 609161.

37. Jaiswal, A., et al., *Lin28B Regulates Angiotensin II-Mediated Let-7c/miR-99a MicroRNA Formation Consequently Affecting Macrophage Polarization and Allergic Inflammation.* 2020. **43**(5): p. 1846-1861.
38. Zhou, S., et al., *Angiotensin II enhances the acetylation and release of HMGB1 in RAW264.7 macrophage.* Cell Biol Int, 2018. **42**(9): p. 1160-1169.
39. Yang, H., Y. Chen, and C. Gao, *Interleukin-13 reduces cardiac injury and prevents heart dysfunction in viral myocarditis via enhanced M2 macrophage polarization.* Oncotarget, 2017. **8**(59): p. 99495-99503.
40. Xu, X., H. Li, and C. Xu, *Structural understanding of T cell receptor triggering.* Cell Mol Immunol, 2020. **17**(3): p. 193-202.
41. Duftner, C., et al., *High prevalence of circulating CD4+CD28- T-cells in patients with small abdominal aortic aneurysms.* Arterioscler Thromb Vasc Biol, 2005. **25**(7): p. 1347-52.
42. Zhou, H.F., et al., *CD43-mediated IFN-γ production by CD8+ T cells promotes abdominal aortic aneurysm in mice.* J Immunol, 2013. **190**(10): p. 5078-85.
43. Sakata, N., et al., *IgG4-positive plasma cells in inflammatory abdominal aortic aneurysm: the possibility of an aortic manifestation of IgG4-related sclerosing disease.* Am J Surg Pathol, 2008. **32**(4): p. 553-9.
44. Siasos, G., et al., *The Role of Endothelial Dysfunction in Aortic Aneurysms.* Curr Pharm Des, 2015. **21**(28): p. 4016-34.
45. Sun, J., et al., *Endothelium as a Potential Target for Treatment of Abdominal Aortic Aneurysm.* 2018. **2018**: p. 6306542.
46. Gurung, R., et al., *Genetic and Epigenetic Mechanisms Underlying Vascular Smooth Muscle Cell Phenotypic Modulation in Abdominal Aortic Aneurysm.* 2020. **21**(17).
47. Enzerink, A. and A. Vaheri, *Fibroblast activation in vascular inflammation.* J Thromb Haemost, 2011. **9**(4): p. 619-26.
48. Unterleuthner, D., et al., *Cancer-associated fibroblast-derived WNT2 increases tumor angiogenesis in colon cancer.* Angiogenesis, 2020. **23**(2): p. 159-177.
49. Sakata, N., et al., *Possible involvement of myofibroblast in the development of inflammatory aortic aneurysm.* Pathol Res Pract, 2007. **203**(1): p. 21-9.
50. Yuda, A., et al., *Effect of CTGF/CCN2 on osteo/cementoblastic and fibroblastic differentiation of a human periodontal ligament stem/progenitor cell line.* J Cell Physiol, 2015. **230**(1): p. 150-9.
51. Fu, Y., et al., *Cartilage oligomeric matrix protein is an endogenous β-arrestin-2-selective allosteric modulator of AT1 receptor counteracting vascular injury.* 2021. **31**(7): p. 773-790.
52. Liu, Z., et al., *Thrombospondin-1 (TSP1) contributes to the development of vascular inflammation by regulating monocytic cell motility in mouse models of abdominal aortic aneurysm.* Circ Res, 2015. **117**(2): p. 129-41.

53. Krishna, S.M., et al., *High serum thrombospondin-1 concentration is associated with slower abdominal aortic aneurysm growth and deficiency of thrombospondin-1 promotes angiotensin II induced aortic aneurysm in mice.* Clin Sci (Lond), 2017. **131**(12): p. 1261-1281.
54. Pagano, M.B., et al., *Complement-dependent neutrophil recruitment is critical for the development of elastase-induced abdominal aortic aneurysm.* Circulation, 2009. **119**(13): p. 1805-13.
55. Harkin, D.W., et al., *Complement C5a receptor antagonist attenuates multiple organ injury in a model of ruptured abdominal aortic aneurysm.* J Vasc Surg, 2004. **39**(1): p. 196-206.
56. Carmo, M., et al., *Alteration of elastin, collagen and their cross-links in abdominal aortic aneurysms.* Eur J Vasc Endovasc Surg, 2002. **23**(6): p. 543-9.
57. Mura, M., et al., *Osteopontin lung gene expression is a marker of disease severity in pulmonary arterial hypertension.* Respirology, 2019. **24**(11): p. 1104-1110.
58. Xin, H., et al., *Calcified decellularized arterial scaffolds impact vascular smooth muscle cell transformation via downregulating α-SMA expression and upregulating OPN expression.* Exp Ther Med, 2019. **18**(1): p. 705-710.
59. Francavilla, C., et al., *Neural cell adhesion molecule regulates the cellular response to fibroblast growth factor.* J Cell Sci, 2007. **120**(Pt 24): p. 4388-94.
60. Bry, M., et al., *Vascular endothelial growth factor-B in physiology and disease.* Physiol Rev, 2014. **94**(3): p. 779-94.
61. Hagberg, C.E., et al., *Vascular endothelial growth factor B controls endothelial fatty acid uptake.* Nature, 2010. **464**(7290): p. 917-21.
62. Zhang, Z.B., et al., *Perivascular Adipose Tissue-Derived PDGF-D Contributes to Aortic Aneurysm Formation During Obesity.* 2018. **67**(8): p. 1549-1560.
63. Cassis, L.A., et al., *ANG II infusion promotes abdominal aortic aneurysms independent of increased blood pressure in hypercholesterolemic mice.* Am J Physiol Heart Circ Physiol, 2009. **296**(5): p. H1660-5.

Tables

Table.1 Echocardiographic and biometric parameters of the experimental mice

	Control (N=15)	AAA (N=14)	P-Value
Rate of AAA model%	0%	78.57%	**P<0.0001
EF%	59.16±5.95	62.75±5.59	0.661
FS%	31.69±5.96	33.69±6.19	0.757
LV Mass (mg)	110.53 (90.45)	127.77 (113.79)	0.324
LVEDV (ml)	62.87 (48.90)	58.58 (51.80)	0.392
LVESV (ml)	25.01 (13.72)	24.14 (14.04)	0.931
Intima thickness (mm)	0.124±0.011	0.178±0.024	*0.0119
Resistance index	0.656±0.043	0.802±0.080	0.0501

AAA: abdominal aortic aneurysm, EF: ejection fraction, FS: shortens fraction, LV: left ventricle, LVEDV: left ventricular end diastolic volume, LVESV: left ventricular end systolic volume. *P<0.05, **P<0.01.

Figures

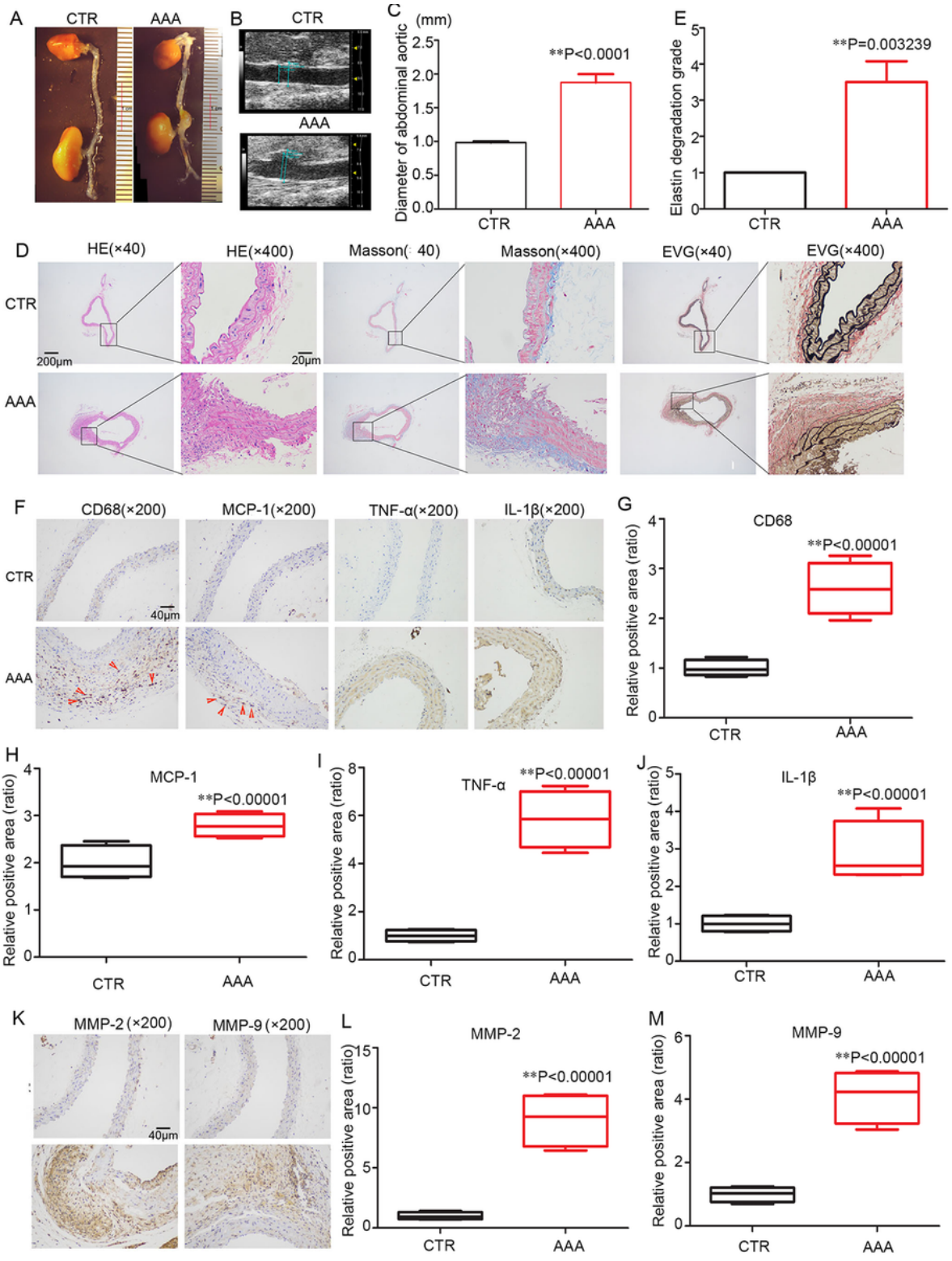

Figure 1

Histological and pathological alternations of Ang II-induced AAA model in mice. (A) Overall morphology of mouse aorta under stereomicroscopy. (B) Vascular ultrasound showed that dilation appeared on the aorta upper the renal artery after Ang II pumping. (C) Statistical quantitative analysis of vessel inner diameter and external diameter. (D) HE, Masson and EVG staining were used to evaluate vascular remodeling, extracellular matrix hyperplasia and degradation of elastic fibers. (E) Semi-quantitative

assessment of the degradation of elastic fibers. (F) The expression of macrophages (CD68 and MCP-1) and inflammatory cytokines (TNF-α and IL-1β) were determined by immunohistochemistry, red arrow: CD68/MCP-1 positive cells (G-J) Semi-quantitative assessment of the expression of CD68, MCP-1, TNF-α and IL-1β. (K) The expression of MMP-2 and MMP-9 in arterial tissue. (L-M) Quantitative assessment of expression of MMP-2 and MMP-9. *P<0.05, **P<0.01.

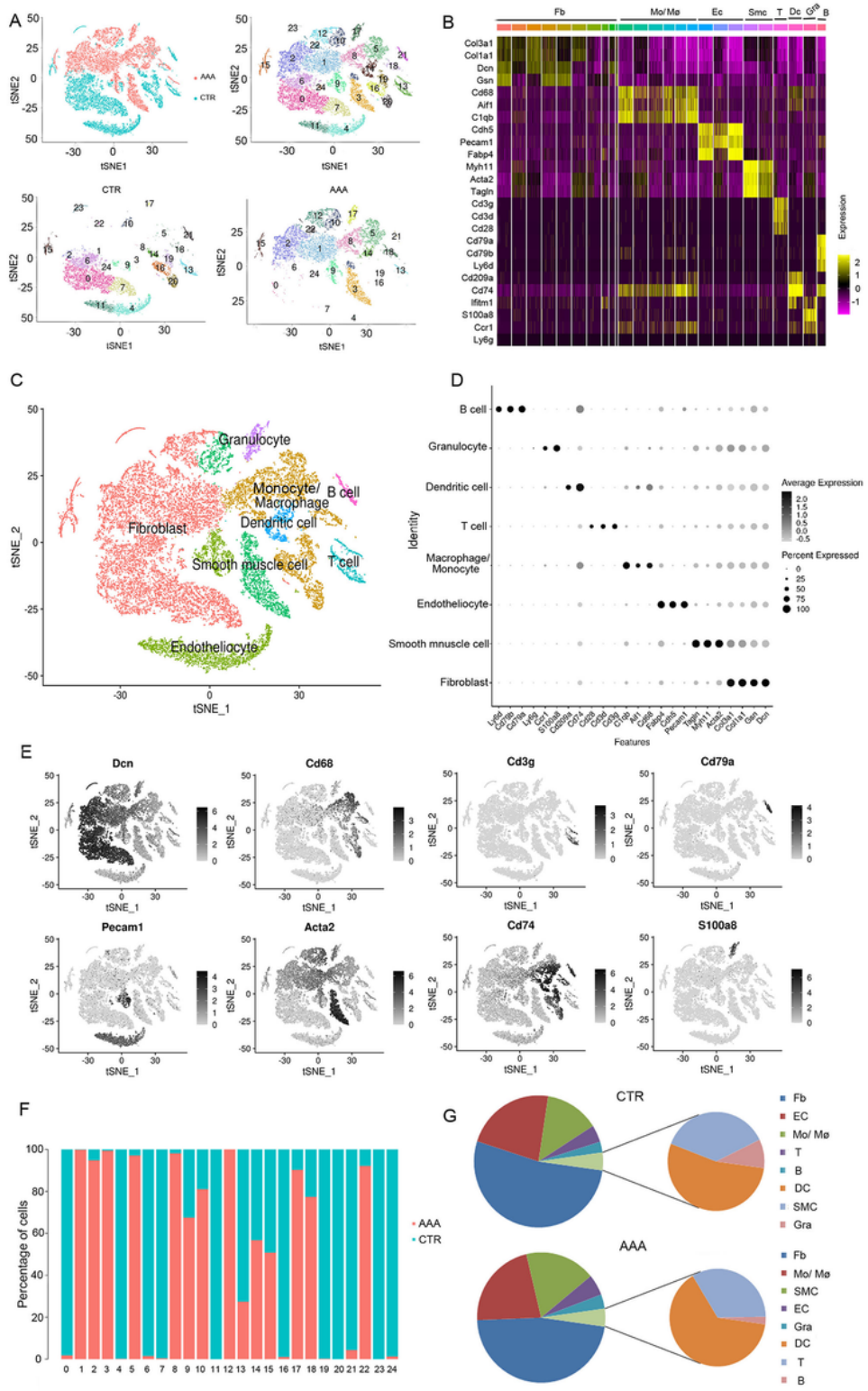

Figure 2

Distribution of cell subpopulations and identification of cell types. (A) The t-SNE plot of renal abdominal aortic tissue from CTR and AAA group. Upper left: the t-SNE plot based on sample distribution, Upper right: the t-SNE plot based on cell cluster distribution. Lower left: the t-SNE plot based on cell cluster distribution in CTR group, Lower right: the t-SNE plot based on cell cluster distribution in AAA group. (B) The heatmap representing the marker genes of different cell types. (C) The t-SNE plot revealed cell types of renal abdominal aortic tissue in both groups. Different colors represented different types of cells. (D-E) The high-light t-SNE (D) and dot plot (E) of selected marker genes. (F) The proportion of the same cluster of cells in different samples. (G) The proportion of different cell types in AAA and CTR groups.

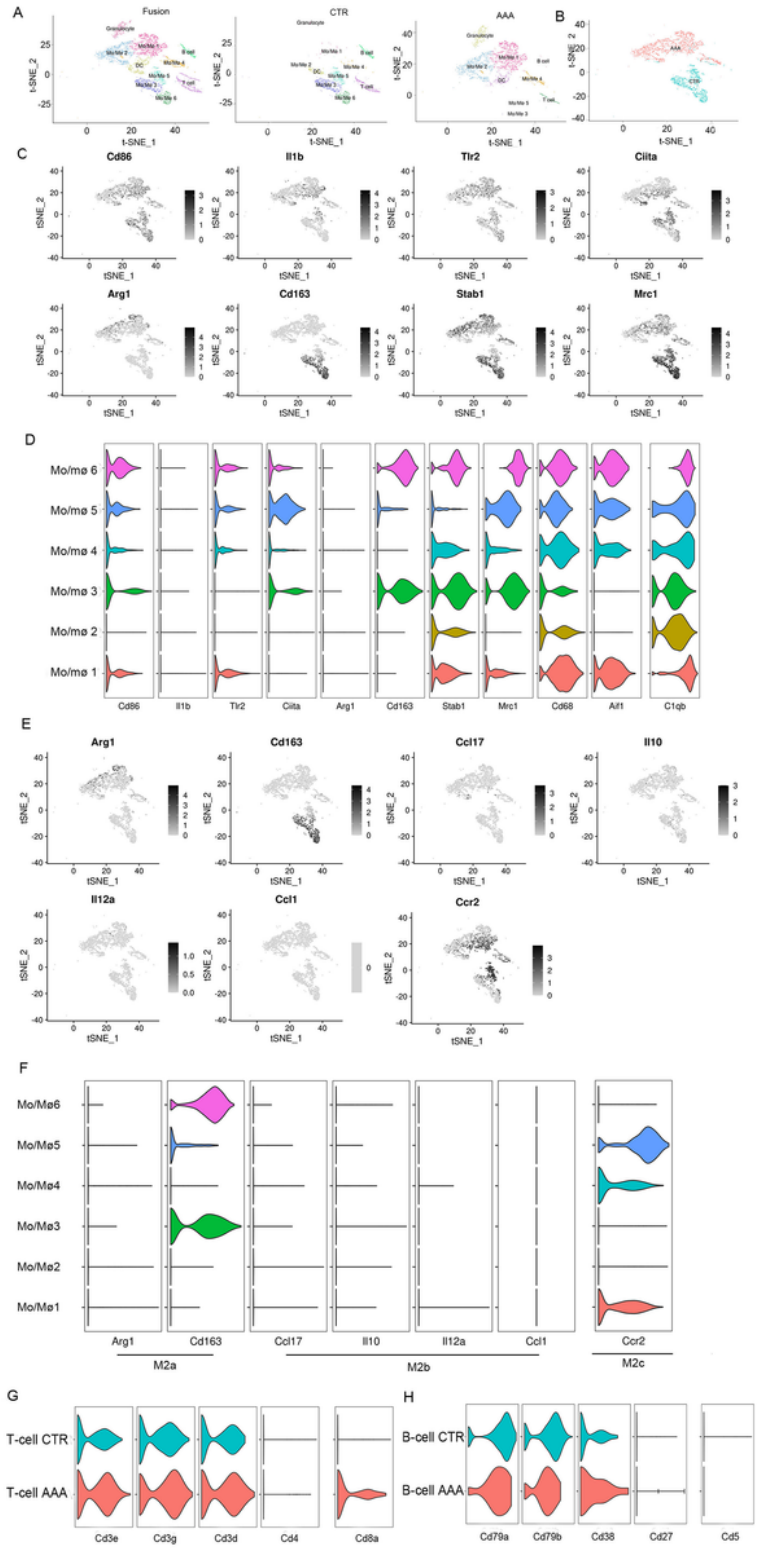

Figure 3

The functional and phenotypic alternations of inflammatory cells during the development of AAA. (A) Different inflammatory cell clusters of abdominal aortic tissue in different condition. Different colors represent different clusters of cells. Left: Cell clusters in fusion condition, Middle: Cell clusters in CTR group, Right: Cell clusters in AAA group. (B) The t-SNE dot plot of Monocyte-macrophages in renal abdominal aortic tissue in different samples. Different colors represent different samples of cells. (C) The

high-light t-SNE plot of selected polarization marker genes. Marker genes of M1 type macrophages: Cd86, IL-1b, Tlr2 and Ciita. Marker genes of M2 type macrophages: Arg1, Cd163, Stab1 and Mrc1. (D) Semi-quantitative evaluation the expression of polarization marker genes by violin plot. (E) The high light t-distributed Stochastic Neighbor Embedding (t-SNE) plot of M2-type macrophage marker genes. (F) The Semi-quantitative evaluation of the expression of type M2 macrophages marker genes according violin plot. (G) The violin plot was used to evaluate the expression of Cd4+T cells and Cd8+T cells during the formation of AAA. (H) The violin plot was used to evaluate the expression of plasmacytes in during formation of AAA. Marker genes of plasmacyte: Cd38+, Cd27+ and Cd5-.

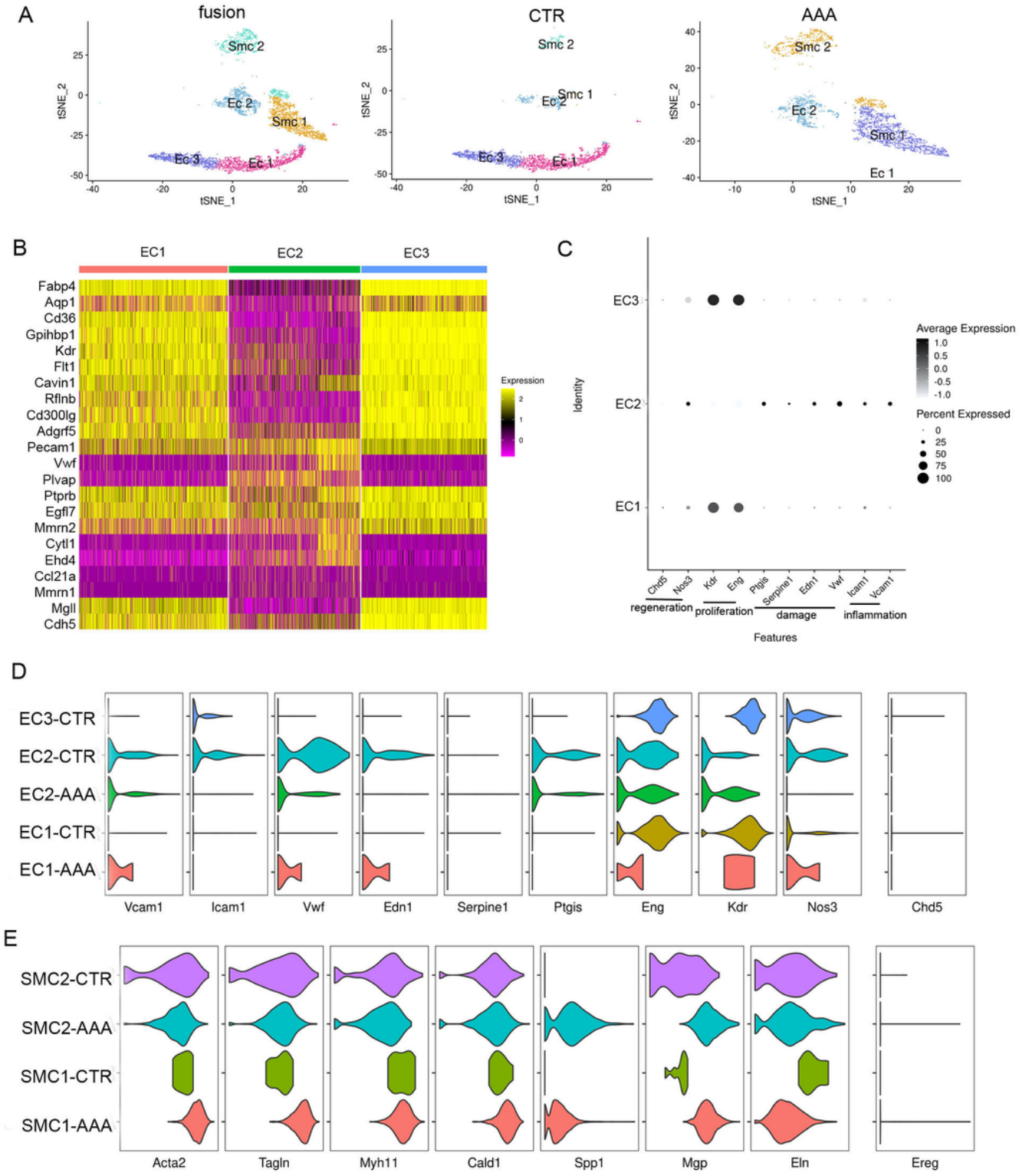

Figure 4

The phenotypic and functional changes in SMC and EC in the formation of AAA. (A) Cell clusters of SMCs and ECs clusters in different condition. Different colors represent different clusters of cells. Left: Cell clusters in fusion condition, Middle: Cell clusters in CTR group, Right: Cell clusters in AAA group. (B) The heatmap of top 10 marker genes of each EC clusters. (C) The dot plot revealed expression of marker genes associated with different functions during AAA formation. (D) Semi-quantitative evaluation the

expression of marker genes by violin plot. (E) The violin plot revealed transformation of contractile SMCs to secretory SMCs.

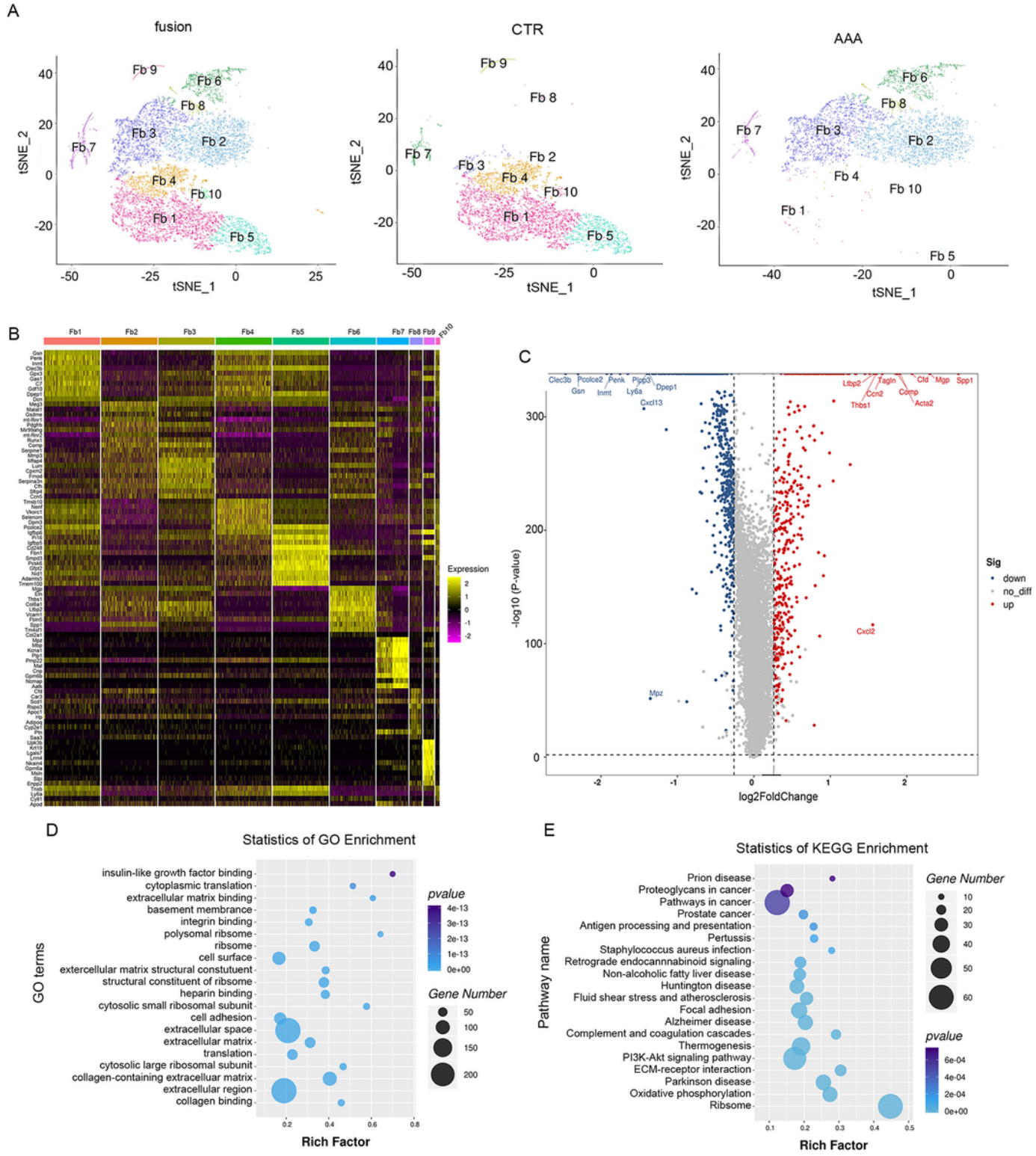

Figure 5

The differential expressed genes (DEGs) analysis of Fbs during AAA formation (A) Cell clusters of Fbs clusters in different condition. Different colors represent different clusters of cells. Left: Cell clusters in fusion condition, Middle: Cell clusters in CTR group, Right: Cell clusters in AAA group. (B) The heatmap of

top 10 marker genes identified for each Fb cluster relative to all other clusters. (C) The volcano plot of differential expressed genes of Fbs between AAA and CTR group. Red dots represent up-regulated genes while blue dots represent down-regulated genes. (D) GO enrichment analysis of differential expressed genes. (E) KEGG pathway enrichment analysis of differential expressed genes.

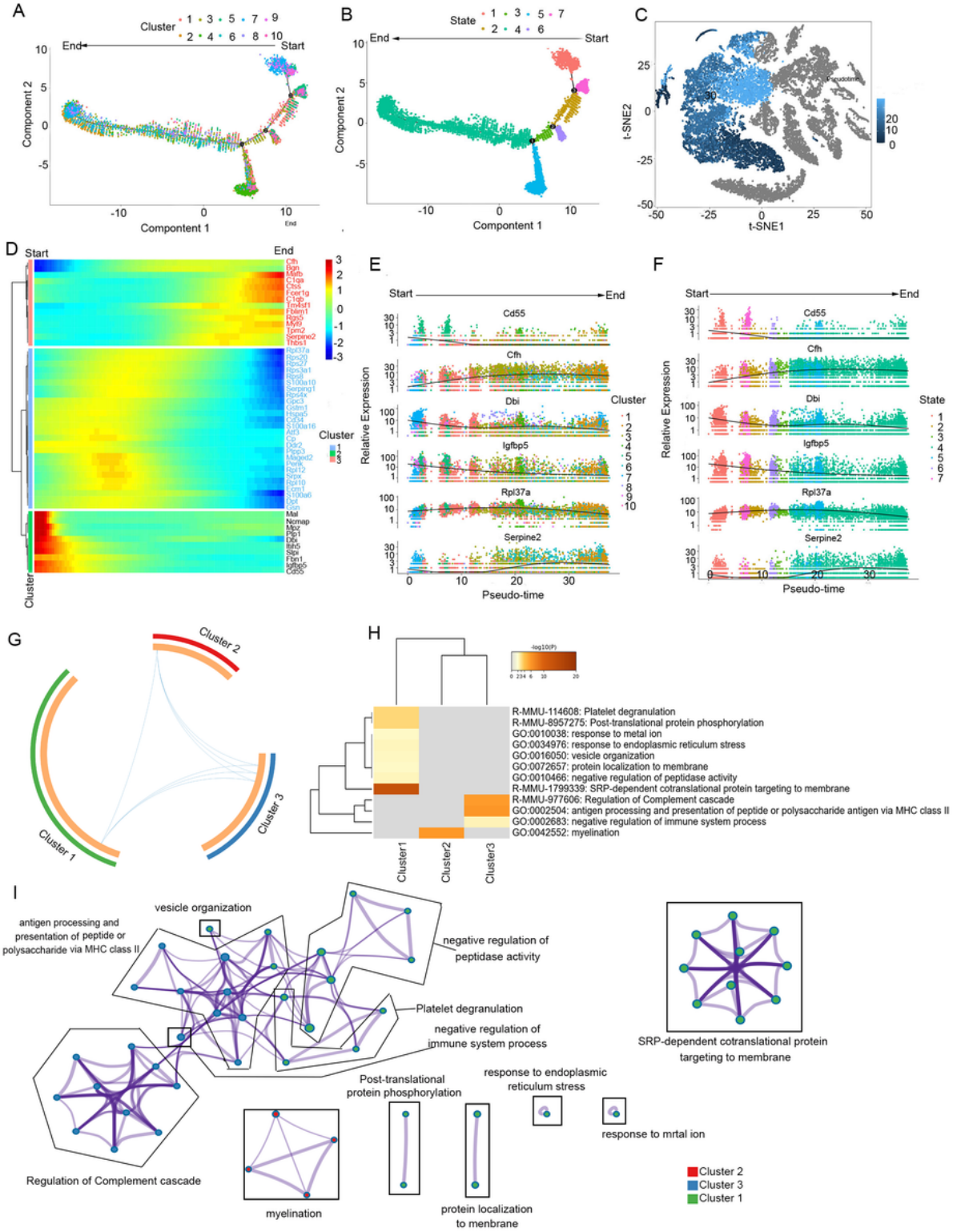

Figure 6

Single cell trajectory revealed the transformation of Fbs during AAA formation. (A) Pseudotemporal trajectory of 10 Fbs clusters. Different color represented different clusters of cells. The cell clusters with high proportion of total cells in the CTR group that decreased with the progression of the disease was the initiation of differentiation (Start). Oppositely the cell clusters with high proportion of total cells in the AAA group that increased with the progression of the disease was the destination of differentiation (End). (B) The pseudotime trajectory was divided into 7 diferent states by Monocle2. Different colors represented different states of cells. From state 1 to state 4 was the main direction of differentiation. (C) The mapping t-SNE plot reflected the direction of Fbs differentiation. The cell differentiation was from dark color cells to light color cells. (D) The heatmap of top 50 genes which had most critical influences on cell transformation. All 50 genes were divided into 3 clusters, Cluster 1: The expression of genes increased first and then decreased. Cluster 2: The expression of the gene was always in a state of decline. Cluster 3: The expression of the gene was always in a state of propradation. (E-F) The expression levels of top 6 gene which had most critical influences on cell transformation were shown over pseudotime by Monocle2. (E) Different colors represent different clusters of cells. (F) Different colors represent different stages of cells.

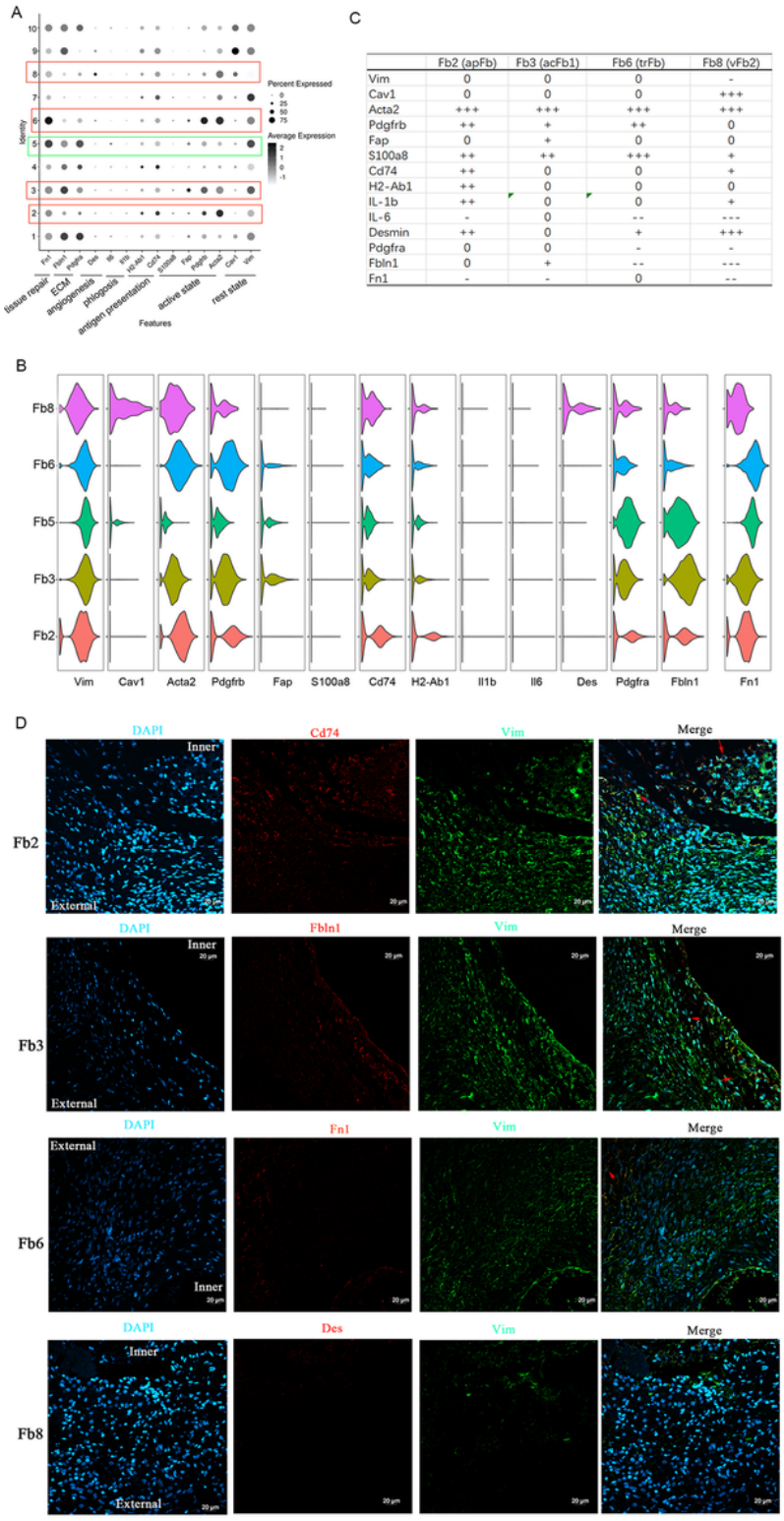

	Fb2 (apFb)	Fb3 (acFb1)	Fb6 (trFb)	Fb8 (vFb2)
Vim	0	0	0	-
Cav1	0	0	0	+++
Acta2	+++	+++	+++	+++
Pdgfrb	++	+	++	0
Fap	0	+	0	0
S100a8	++	++	+++	+
Cd74	++	0	0	+
H2-Ab1	++	0	0	0
IL-1b	++	0	0	+
IL-6	-	0	--	---
Desmin	++	0	+	+++
Pdgfra	0	0	-	-
Fbln1	0	+	--	---
Fn1	-	-	0	--

Figure 7

Identification of 4 increased fibroblasts in function and spatial distribution by analysis of marker genes. (A) The dot plot revealed the characteristics of Fbs in each cluster. Fb5 (in green wireframe) was selected as control. (B) The violin plot semi-quantitatively analyzed the characteristics of Fbs increased during formation of AAA. (C) Increased Fbs during AAA formation was classified according to the different

expression of characteristic genes. (D) The distribution of 4 Fbs in aneurysm tissues identified by immunofluorescence. The red arrow points to the marker genes co-expression cells.

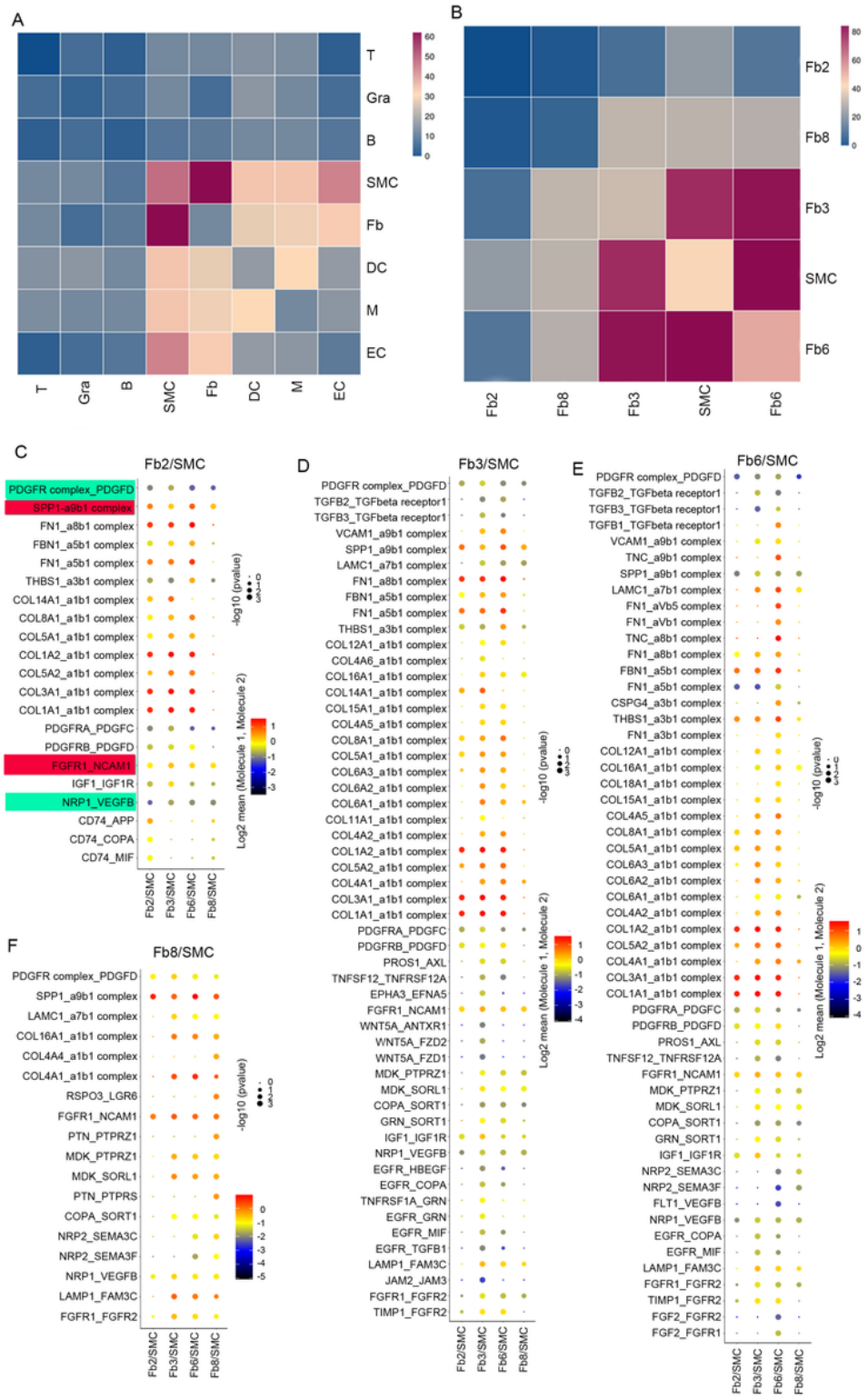

Figure 8

Ligand-receptor analysis between 4 increased fibroblasts and SMCs. (A-B) The heatmap of cellular interactions. (A) The intercellular interactions of 8 different cell types. (B) The intercellular interactions between SMC and 4 increased Fbs (Fb2, Fb3, Fb6 and Fb8). Rows and columns represent cell types, and

each grid represents the number of interactions between cells. The redder the color, the more interactions between cells and the stronger the communication relationship between cells. (C) Reciprocal action between Fb2 and SMC, (D) Reciprocal action between Fb3 and SMC, (E) Reciprocal action between Fb6 and SMC, (F) Reciprocal action between Fb8 and SMC. The ligand receptor pairs shown in green background were low co-expressed, while receptor pairs shown in red background were high co-expressed in the four groups.

Supplementary Files

This is a list of supplementary files associated with this preprint. Click to download.

- SupplementFig.1.tif
- SupplementFig.2.jpg
- SupplementFig.3.jpg
- SupplementFig.4.jpg